

# Performance of Nanoparticle Tracking Analysis in the Measurement of Extracellular Vesicles

Authors: Romina Ayelén Campos

Submitted: 26. October 2025 Published: 24. November 2025

Volume: 12 Issue: 5

Affiliation: University of Buenos Aires, Buenos Aires, Argentina & Albert-

Ludwigs University of Freiburg, Freiburg im Breisgau, Germany

Languages: English

Keywords: Extracellular Vesicles; Nanoparticle Tracking Analysis

Categories: Life Sciences, Medicine, Demetrios Project

DOI: 10.17160/josha.12.5.1102

# Abstract:

Extracellular vesicles (EVs) are membrane-enclosed, non-replicating, submicron-vesicles released by all living cells. Depending on their origin pathway and donor cell, EVs present a specific biomolecular cargo that allows tracing the cell of origin and its status, proposing EVs as potential biomarkers of different diseases, among other clinical applications. Thus, EVs research field is an area of rapid and constant growth. However, the complexity of EVs, based mainly on their heterogeneity in size and cargo, presents unique challenges for their characterization. Nanoparticle Tracking Analysis (NTA) is a technique useful for the quantification and size distribution estimation of nanoparticles in a single particle measurement and is also capable of phenotyping when combined with the fluorescent mode. While the application of NTA in the field of EVs is promising, this technology needs to be improved. On the one hand, the algorithms must be adapted to the heterogeneity of EVs to obtain more accurate measurements. On the other hand, the low refractive index of EVs (a feature with direct impact on the results by optical methods such as NTA) leads to the need of suitable reference materials (RM) for instrument calibration. The aim of this project is to



Journal of Science, Humanities and Arts

JOSHA is a service that helps scholars, researchers, and students discover, use, and build upon a wide range of content

mon macmore precioe	maniomanoar aige	manno aro rogano.	a to train romout the	,	· O.







# "Performance of Nanoparticle Tracking Analysis (NTA) in the measurement of Extracellular Vesicles (EVs)"

For the degree of Master of Sciences

Author: Romina Ayelén Campos

Cohort: 2021 - 2023

Director: Prof. Dr. Irina Nazarenko

Co- Director: Prof. Dr. Timoteo Marchini

Direct Supervisor: Prof. Dr. Irina Nazarenko

Faculty of Pharmacy and Biochemistry, Faculty of Medicine –

Universidad de Buenos Aires, Argentina

Faculty of Medicine –

Albert Ludwigs University of Freiburg, Germany

2023







Author: Romina Ayelén Campos

Director: Prof. Dr. Irina Nazarenko

Co- Director: Prof. Dr. Timoteo Marchini







# Master of Science in Biomedical Sciences Statement for the Master's Thesis

Hereby I confirm that			
I completed the submitted mas	ter's thesis independently.		
I used no sources or aids other than those stated and all verbatim or conceptual content taken from other works has been identified as such.			
The submitted master's thesis subject of another examination		in large part the	
The electronic version of the m the same as the printed version		n content and format	
The master's thesis has not yet been published.			
Freiburg, 20.01.2023	Romina Ayelén Campos		
Place, date	Name, First name	Signature	



**Date** 



Hereby I declare on oath that I wrote my Master Thesis myself and did not use other sources than



mentioned as resources. Freiburg, 20.01.2023 Romina Ayelén Campos Place, date Name, First name Signature The Master Thesis can be accessible to the public 24 months after the completion of the procedure. 20.01.2023\_\_\_\_\_ Signature of the student Name: Romina Ayelén Campos Date 20.01.2023\_\_\_\_ Name: Prof. Dr. Irina Nazarenko Signature of the Director **Date** Name: Prof Dr. Timoteo Marchini 20.01.2023\_\_\_\_\_ Signature of the Co-Director

#### **ABSTRACT**

Extracellular vesicles (EVs) are membrane-enclosed, non-replicating, submicron-vesicles released by all living cells. Depending on their origin pathway and donor cell, EVs present a specific biomolecular cargo that allows tracing the cell of origin and its status, proposing EVs as potential biomarkers of different diseases, among other clinical applications. Thus, EVs research field is an area of rapid and constant growth. However, the complexity of EVs, based mainly on their heterogeneity in size and cargo, presents unique challenges for their characterization.

Nanoparticle Tracking Analysis (NTA) is a technique useful for the quantification and size distribution estimation of nanoparticles in a single particle measurement and is also capable of phenotyping when combined with the fluorescent mode. While the application of NTA in the field of EVs is promising, this technology needs to be improved. On the one hand, the algorithms must be adapted to the heterogeneity of EVs to obtain more accurate measurements. On the other hand, the low refractive index of EVs (a feature with direct impact on the results by optical methods such as NTA) leads to the need of suitable reference materials (RM) for instrument calibration.

The aim of this project is to evaluate the performance of NTA for the measurement of heterogeneous populations of EVs. Firstly, SiO2 nanoparticles were used as RM and the standard operating procedures (SOPs) were established for their measurement according to their size. Once established, the SOPs were used for the measurement of different sizes of RM, and EVs derived from cell culture. Our results indicate that to cover the full spectrum of EVs sizes, three SOPs are needed: SOP50 (for the measurements of smaller EVs: 30 - 80nm), SOP100 (80 - 200nm), and SOP500 (200-500). Secondly, the performance of the NTA in fluorescent mode was evaluated for the measurement of synthetic EVs with different fluorophore densities, evidencing that this mode of the instrument depends on the fluorescence intensity regardless of the size of the particle analyzed. Finally, the size of the particles included in this work was measured direct using transmission electron microscopy (TEM).

This work details a deep analysis of the performance of NTA, providing valuable data that can be used for the generation of user guidelines for the standardization of EVs characterization. Although more experiments will be necessary to establish determinative conclusions, it is likely that more precise mathematical algorithms are required to truly reflect the heterogeneity of EVs.

# ACKNOWLEDGMENTS.

First, I would like to thank my thesis director and direct supervisor, Prof. Dr. Irina Nazarenko, for giving me the opportunity to carry out this work and grow by her side, and Tanja Gainey Schleicher for taking care of me during my first steps in the lab, teaching me both with infinite patience due to my inexperience in basic research. I always felt part of the work team and that my opinion was valuable. Thanks to my co-director, Prof. Dr. Timoteo Marchini, who was always open to advise and accessible to help me.

I also want to thank my other collaborative teammates Melanie Schwaemmle,

Maren Voglstaetter, and Iana Tarakanchikova, who have made my job easier so many
times.

I feel very grateful to the entire IMBS team. The directors of the program, Prof. Dr. Christoph Borner and Prof. Dr. Marta Mollerach, both were always accessible to assist my academic and personal growth. I thank the secretaries Belén Moyano, Ana Cortés, and Bärbel Schätzle, for their infinite help.

I also appreciate the contribution of my scholarships, provided by the UBA, CUAA, DAAD, and Fundación BioThera. Without their help, this would not have been possible for me. In addition, I thank all my fellow IMBS members for their companionship along this path, many of whom have become my friends today, which I believe is the most valuable title one can have. It was fortunate to coincide in this experience with such excellent professionals... but more importantly: excellent people.

I thank Julian, for his patience and infinite support, who has encouraged me to continue when I felt frustrated and to trust myself when many times I do not. I am so happy to have met you. And last but not least, I would like to thank my family for their support and for being happy to see me go after my dreams, even if it means having me far away... To my father: I hope you are proud of my achievements but more important... I hope you are proud of the person I have become. I miss you every day.. And the most important person in the world, my mother: Sos el lujo de mi vida.

Que cada vez que llores, Lo sabrá mi corazón, Y no nos encontraremos, Pues siempre estuve a tu lado, Hacia dónde y hasta cuándo... Esas son cosas de Dios.

Fragment of the song: "If I go before you" (Si me voy antes que vos), Jaime Roos

# **LIST OF ABBREVIATIONS**

Automatic fraction collector
bicinchoninic acid
endosomal sorting complexes required for transport
Extracellular vesicle
Fraction
Major histocompatibility complex
Messenger RNA
microRNA
Multivesicular body
Nanoparticles tracking analysis
Phosphate-buffered saline
IZON qEVoriginal / 35nm Column
Standard deviation
Size exclusion chromatography
Stantard Operating Procedure/Stantard Operating Procedures
Tangential flow filtration
Ultracentrifugation
Void volume

# CONTENT

INTRODUCTION	9
1. Overview of EVs research field.	9
1.1 What are EVs and why are they so important?	9
1.2 Structural characteristics and classification of EVs	9
1.3 EVs composition: Internal cargo and surface molecules	10
1.4 Biological function: role in intercellular communication	12
1.5 Potential applications and challenges in the field	14
2. Nanoparticle tracking analysis	18
3. Reference materials in the EVs research field	20
AIM OF THIS PROJECT	22
MATERIALS AND METHODS	23
Materials	23
Methods	27
RESULTS AND DISCUSSION	40
Measurement of reference material and EVs using NTA in scatter mode	40
1.1 SOPs establishment for measurement of SiO2 nanoparticles of determined sizes	40
1.2 Calculation of the correction factor for each SOP established	42
1.3 SOPs cross-compatibility evaluation	45
1.4 Measurement of 30, 50, 70, and 150 nm particles using the established SOPs	52
1.5 EVs measurement using the established SOPs	55
1.6 Determination of total protein contained in the isolated samples	59
2. Measurement of reference material and EVs using NTA in fluorescent mode	60
2.1 Establishment of the SOP in fluorescent mode	60
2.2 Relative correction factor calculation	60
2.3 Measurement of synthetic vesicles of different fluorophores densities	62
3. Assessment of size determination by transmission electron microscopy	66
CONCLUSIONS	71
REFERENCES	72

#### INTRODUCTION

# 1. Overview of EVs research field.

# 1.1 What are EVs and why are they so important?

The term "Extracellular Vesicles" (EVs) includes a diverse group of nonreplicating lipid bilayer particles released by all living cells, including eukaryotes and prokaryotes. EVs are released into the extracellular environment from the donor cell under physiological or pathological conditions, not only when activated, but also in their basal state or even when undergoing apoptosis (Willms et al. 2018; Yáñez-Mó et al. 2015). They are found in most biofluids, including blood, urine, cerebrospinal fluid (CSF), saliva, tears, and breast milk (Raposo and Stoorvogel, 2013).

Not long ago, EVs were considered membrane debris and their biological function was unknown. In 1946, EVs were reported (probably for the first time in the literature) not as "EVs" but as procoagulant platelet-derived particles in normal plasma, isolated by high-speed centrifugation (Chargaff and West, 1946). In 1967 it was shown that fresh plasma released from intact platelets contained nanometric particulate matter rich in phospholipids, which could be separated by ultracentrifugation. Although this opportunity the isolated material was called "platelet-dust", it was shown that a large part of this material showed coagulant properties (Wolf, P. et al. 1967). It was almost 20 years later, in 1983, when was demonstrated that transferrin receptors in reticulocytes were internalized into small vesicles of approximately 50nm diameter, and then released intact in the extracellular space (C. Harding et al., 1983). A few years later, Rose Johnstone first gave these vesicles the name exosomes (Johnstone et al., 1987). However, it was not until 1996 that Raposo and colleagues (Raposo et al., 1996) discovered that dendritic cells produce EVs that carry on their surface the major histocompatibility complex MHCII, in its peptide-bound conformation and demonstrated the functionality of EV-bound MHCII, as B-lymphocyte-derived EVs induced an MHCI-antigenspecific T-cell response, demonstrating for the first time a biological function of EVs.

Measurement of the size and concentration of the EVs provides crucial information, since these parameters are determined by the pathway of origin and the state of the cells of origin respectively. Nowadays, it is well known that EVs are involved in a regulated mechanism of intercellular communication by transporting relevant molecular cargo from a donor cell to a recipient cell. In addition, the specific pattern of proteins and nucleic acids that EVs present is dependent on their cell of origin, which allows them to be traced back to the donor cell and its status (Nazarenko et al. 2010; Nazarenko 2020; Yáñez-Mó et al. 2015).

Since then and to date, the EVs research field has grown exponentially and has expanded through different branches of science, trying to understand the mechanisms underlying the

pathways involved in their biogenesis, how this affects their composition, and the possible novel clinical applications of EVs (as biological markers of a plethora of pathophysiological processes in the health-disease process, as well as monitoring, prognosis, and treatment). Due to what has been mentioned, the interest in detailed knowledge about EVs continues to develop year after year.

# 1.2 Structural characteristics and classification of EVs

EVs share certain similar structural characteristics: they are enveloped by a lipid membrane, within a defined size range, and present (in their interior and on their surface) different types of biomolecules found in the respective donor cells (Möller, A., & Lobb, R. J. 2020; Nazarenko et al. 2020). However, they vary in size, internal biochemical content and molecular surface composition, and the biogenesis pathways involved in their formation. The knowledge of the scientific community is still exceeded by the immense variability of EVs and limits the existence of a definitive classification of the different EV subpopulations, which is constantly updated (Margolis & Sadovsky, 2019).

There are at least three aspects underlying the heterogeneity of EVs: The characteristics that their cell of origin (donor cell) transfers to them, as well as the mechanisms involved in their biogenesis and subsequent release from donor cells. Three different cellular pathways by which vesicles can be released have been identified to date, which allowed a more adequate nomenclature and classification based on their size and mechanism of formation, which in turn, confers the corresponding EVs characteristics. and unique properties (Doyle and Wang 2019; M. H. Vasconcelos et al. 2020).

- Exosomes: Their size varies from 40 to 120 nm in diameter, are originated in the endolysosomal system and released into the extracellular space through multivesicular bodies (MVB). MVB originate from early endosomes which are formed by the internal budding of the plasma membrane of cells. In its formation process, the endosomal membrane invaginates, forming intraluminal vesicles that contain cytoplasmic proteins, lipids, and nucleic acids (El Andaloussi et al. 2013; Doyle and Wang 2019), with the possibility of having different destinations: fusing with the lysosome membrane, causing their degradation and or fuse with the plasmatic membrane of the cell causing the release of exosomes into the extracellular space (Yáñez-Mó et al. 2015; Simons und Raposo 2009; Théry et al. 2009).

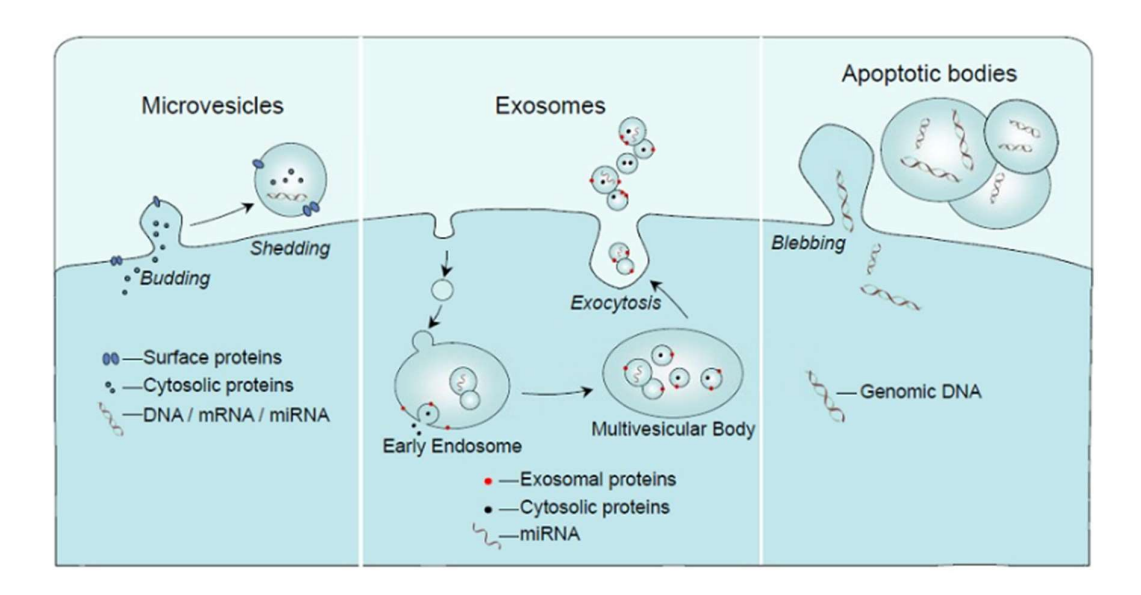


Figure 1: Biogenesis pathways of EV subtypes. Exosomes are released upon the fusion of multivesicular bodies with the plasma membrane. Microvesicles are formed by budding of the plasma membrane and apoptotic bodies are formed by blebbing of the plasma membrane of dying cells (image taken from Journal of Endocrinology 228 R57-R71 2016).

- Microvesicles: Microvesicles or ectosomes are medium-sized vesicles, their size ranges between 100 and 1000 nm, and they are formed by sprouting from the plasma membrane of cells and released into the extracellular space (Zaborowski et al. 2015; Yáñez- Mó et al. 2015), through a process that is believed to require different components of the cytoskeleton, such as actin and microtubules, as well as molecular motors and fusion machinery (Doyle und Wang 2019; Cai et al. 2007). In the same way that exosomes, microvesicles contain cytoplasmic proteins, lipids, and nucleic acids from their cell of origin, due to their formation mechanism (El Andaloussi et al. 2013). The number of microvesicles released would depend on the physiological state and microenvironment of the cell of origin (Zaborowski et al. 2015).
- Apoptotic bodies: They represent the largest group of EVs, between 500 nm to 2 μm in diameter (Willms et al., 2018), and unlike the other types, they are not formed by secretion from the donor cell, but by a rearrangement of the cytoskeleton with the consequent formation of blebs on the cell membrane during apoptosis (El Andaloussi et al. 2013). After their formation, apoptotic bodies are phagocytosed by neighboring cells or macrophages. Due to its formation mechanism, by the disassembly of the cell, it was assumed that apoptotic bodies would be loaded with random cargo, including cell organelles and DNA fragments from the cell of origin (Hashimoto et al. 1998; Ihara et al. 1998), which could later have important effects on the recipient cell (Battistelli & Falcieri, 2020; X. Xu et al., 2019).

# 1.3 EVs composition: Internal cargo and surface molecules

As previously mentioned, since EVs are formed by budding or bleb formation in the endosomal or plasma membrane, they carry within them a variety of biological information called "cargo", which is directly related to the membrane and cytosol. of the donor cell. The charge will vary according to the cell of origin and the pathophysiological state of the cell and will aid the transfer of new information between cells or the phenotypic modification of the recipient cell after the uptake of the EVs. The most common components are DNA, RNA, proteins, and lipids (Doyle and Wang 2019), which will be involved in various specific biochemical and cellular processes.

The presence of DNA in the cytoplasm of cells is often related to cell damage, infection, or tumor processes, and it is believed that EVs may act as effectors of cellular homeostasis by excreting damaged DNA from the cell (Takahashi et al., 2017). DNA associated with EVs includes single-stranded DNA (ssDNA), double-stranded DNA (dsDNA), and mitochondrial DNA (mtDNA). It represents 90% of the total extracellular DNA or cell-free DN (Fernando et al., 2017). The presence of DNA in EVs is well recognized. However, the underlying mechanisms are poorly understood and currently there is only speculation as to how this occurs. The most popular theory is that EV-DNA originates from damaged DNA in the cytoplasm. However, this would not explain the recruitment of mtDNA or other types of DNA and therefore, more studies are needed (Ghanam et al., 2022).

Despite the wide variety of RNA types found in EVs, only a few classes are functional (O'Brien et al., 2020). The RNA content of EVs differs substantially from that of donor cells (Turchinovich et al., 2019). In EVs, approximately 30-94% of the total is ribosomal RNA (rRNA), and 2-40% of the remaining RNA biotypes. These include small nuclear RNAs (snRNA), small nucleolar RNAs (snoRNA), long noncoding RNAs (lncRNA), mitochondrial RNAs, Y RNAs, vault RNAs (vtRNAs), and mature microRNAs (miRNAs). Of these, the greatest clinical relevance is presented by RNAs with known functions when taken up by receptor cells (miRNAs, mRNAs, and snoRNAs) since they can be used to study the participation of EVs in different physiological or pathological processes (O'Brien et al., 2020). For example, while miRNAs can downregulate the expression of target genes, mRNAs can be functionally translated in the target cell (Teng und Fussenegger 2020).

Lipids are essential molecular components of EVs, not only for their structural functions as part of their lipid bilayer, but also as regulators during EV biogenesis, release, targeting, and cellular uptake (Donoso-Quezada et al., 2021). Although everything is influenced by the type and physiological state of the donor cell (Carayon et al., 2011; Llorente et al., 2013), quantitatively, we can find a relative abundance of lipids such as cholesterol, sphingomyelin, glycol-phospholipids, gangliosides, and phosphatidylserine, compared to donor cells (Skotland et al., 2017).

Regarding the protein content, EVs can present specific receptors for antigen presentation (MHC class I and II), costimulatory molecules such as CD83 and CD40, cytokines together with their specific receptors (tumor necrosis factor alpha (TNF-α), and receptor tumor necrosis factor alpha (TNFαR)), and death receptor ligands, including FASL or TRAIL (Gutiérrez-Vázquez, Cristina, et al. 2013; Lu J., et al. 2018; Rodriguez, M. et al. 2011). Since exosome formation and transport of BVM are regulated by endosomal sorting complexes required for transport (ESCRT) as well as their accessory proteins (eg, TSG101, ALIX), exosomes are expected to contain these proteins as well (Théry et al. 2001; Doyle and Wang 2019; Morita et al. 2007).

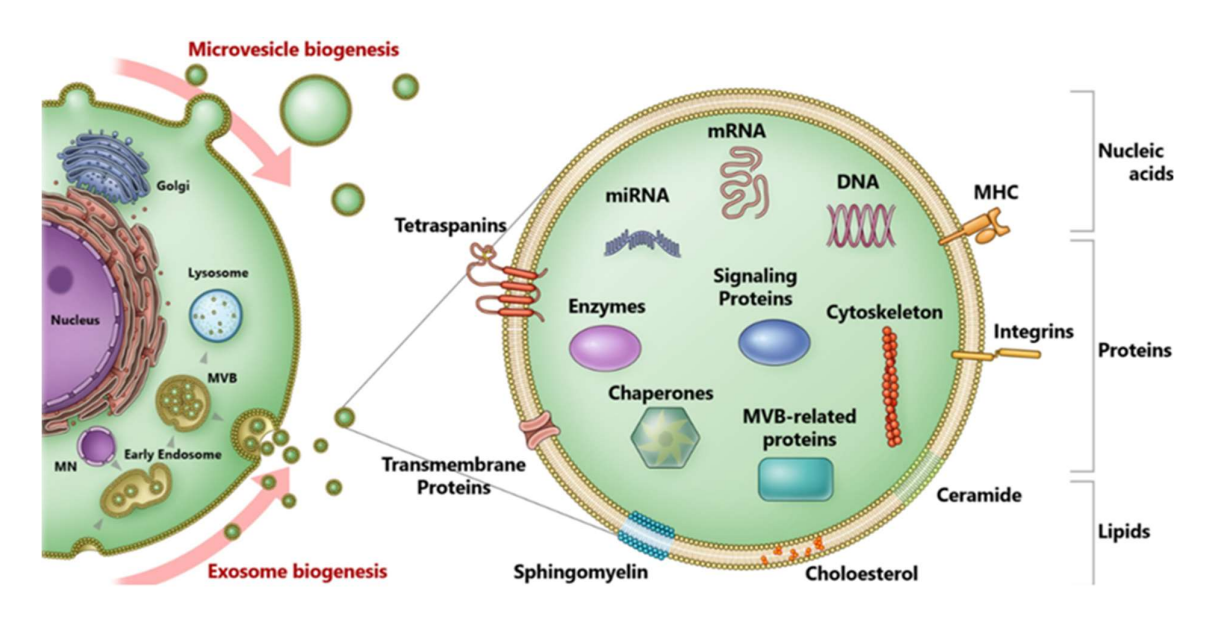


Figure 2: Molecular composition of EVs. EVs contain various components including nucleic acids, proteins, lipids, and metabolites. The components can either be enclosed in or associated with the lipid bilayer of the EV. Most of them are enriched in EVs during the biogenesis whereas some are involved in the biogenesis (image taken from Yokoi, A., & Ochiya, T. et al. 2021.

Despite all this heterogeneity, EVs may contain common proteins that will aid in their further identification; The so-called "vesicle markers", which carry very rich domains of tetraspanins on their surface (Michael Zhuo Wang et al. 2019; Pfafll M.W. et al. 2019). As they are associated with the plasma membrane, they can be found on the surface of EVs (Witwer et al. 2013). At first, these tetraspanins were thought to be unique to exosomes, but they were later identified on the surface of microvesicles and apoptotic bodies (Crescitelli et al. 2013). The exact process of how proteins are packaged into EVs is still unknown to this day, but it is presumed that they have a high affinity for the plasma membrane or bind to anker proteins after different modifications, and therefore remain in the MVB cycle (van Niel et al. 2006). In

humans, the tetraspanin protein family consists of 33 members, 10 interacting with their type and with other cytosolic and membrane proteins to create a unique domain called tetraspanin-enriched microdomains (TEMs). Tetraspanins oversee the mediation of a whole range of processes, including immune activation, cell adhesion, extravasation of tumor and immune cells, regulation of intracellular trafficking, and even virus entry. Evidence suggests that TEMs are an important key in the classification of intraluminal cargo and exosome secretion (Pfafll M.W. et al. 2019; Rodriguez, M. et al. 2011).

Since a few years ago, tetraspanins have been proposed and used as markers to differentiate EV from non-EV isolated particles. The most commonly used are the tetraspanins CD9, CD63, CD81, and CD82. However, it should be noted that not all of these tetraspanins will be expressed concurrently in all EV types, and they are mostly enriched in vesicles than in cell lysates (Michael Zhuo Wang et al. 2019).

# 1.4 Biological function: role in intercellular communication.

After what has been said so far, it is obvious to state that although at first it was believed that the EVs were only responsible for the removal of unnecessary material or cellular debris, their biological function as mediators of intercellular communication was subsequently verified, influencing a large number of physiological and pathological processes (Yuana et al. 2013).

Once released by the donor cell, EVs are taken up by the recipient cell, through a type of intercellular communication known as "horizontal transfer" (Nazarenko et al. 2020). Cargo and cargo release are actively regulated mechanisms and this delivery will result in various biological effects on the recipient cell depending on its content. Three different main mechanisms have been proposed for the uptake of EVs: direct fusion with the plasma membrane, endocytosis, and phagocytosis (Kharaziha et al. 2012). However, they can also be taken up by using membrane nanotubes and tunneling nanotubes, using the gap junctions of the cells, among other mechanisms (Cristina et al. 2013).

As mediators of intercellular communication, through horizontal transfer, EVs have an impact on numerous pathophysiological biological processes. From the physiological point of view, they participate in the immune response, angiogenesis, the development of the nervous system (Simons und Raposo 2009; Keller et al. 2006; Toro et al. 2015), etc. In addition, EVs can transport different forms of nucleic acid to other cells, influencing their gene expression, something that was thought unlikely just a few years ago.

The role of EVs in pathological processes has been widely studied, mainly in the oncology field, not only as promoters of tumor progression (Yang, A.et al. 2022; Peinado et al. 2012) but

also as critical factors for metastasis (Nejati-Koshki, K. et al.2022).and drug resistance (Su, L. et al. 2022). Cancer cells release a significantly higher amount of EV compared to healthy cells, and this has been shown to influence tumor formation, progression, and metastasis (Tickner et al. 2014) through a tightly regulated interaction with the tumor microenvironment and surrounding macrophages (Huang, C. et al. 2022). Regarding chemoresistance, several mechanisms were also studied. On the one hand, drug-resistant tumor cells have been shown to acquire this characteristic by entrapping chemotherapeutic drugs in EVs and excreting them. On the other hand, and as mentioned before, EVs contain a large amount of genetic material and are exchanged between cells in the tumor microenvironment. In this way, drug-resistant tumor cells act on sensitive cells through EV, conferring resistance on them (Li Su et al. 2022). In breast cancer, for example, mtDNA transfer through EVs has been shown to promote resistance to hormone therapy (Cai et al., 2014). In addition, tumoral cells can acquire drug resistance by EVs horizontal transfer of enzymes involved in drug metabolism (Tang, J. H. et al. 2017). Another novel mechanism of tumor resistance involves the regulation of the tumor microenvironment immunity, through the suppression of the immune response and activation of immunosuppressive cells (Graner, M. W. et al. 2015) or the neutralization of pharmacological antibodies through EVs Tumor-derived is another mechanism to reduce antitumor therapeutic efficacy (Zeidler, R. et al. 2011; Pupa, S. M. et al. 2012).

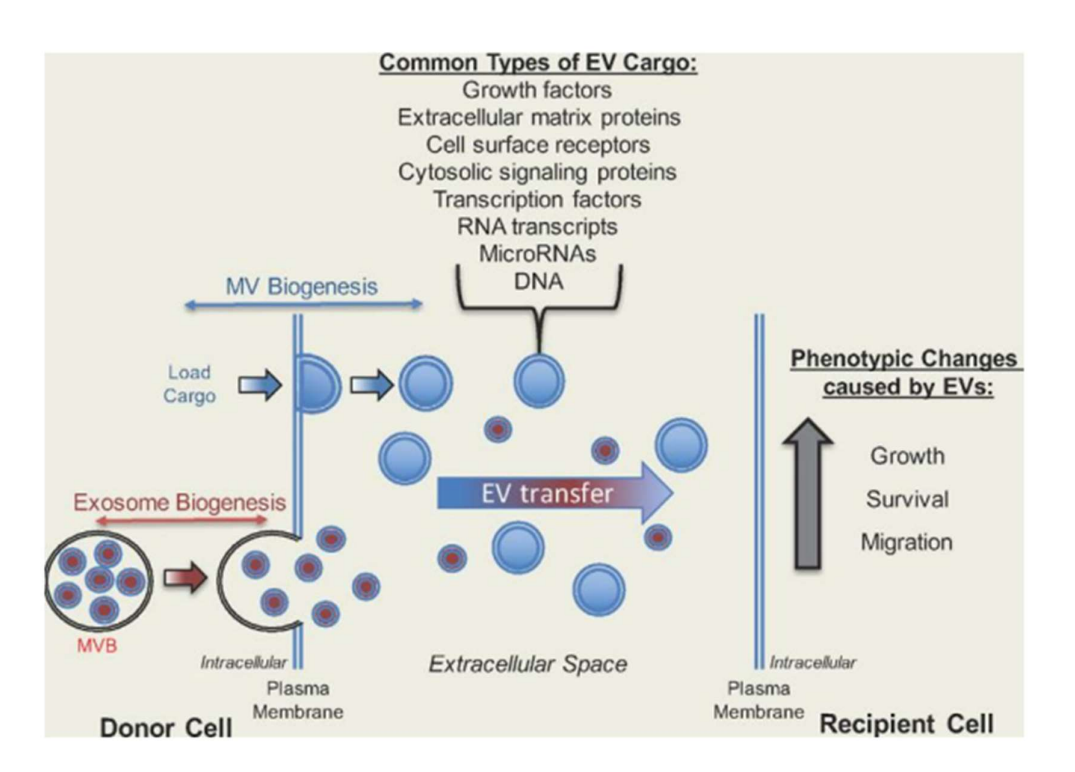


Fig 3. Schematic representation of EVs horizontal transfer. EVs are released by the donor cell into the extracellular space where they will be uptake by the recipient cells to finally induce a phenotypic change within the new cell, which will depend on the EVs composition and state of the donor cell.

Moreover, cancer is not the only pathological process in which the role of EVs has been studied. Their participation in the pathogenesis of autoimmune diseases includes multiple mechanisms. For instance, EVs derived from abnormal regulatory T cells were associated with disease pathogenesis and progression in Psoriasis and Multiple Sclerosis (Guo, J., & Jia, R. 2022; Martínez-Lostao L et al. 2019). Regarding the field of neuropathology, it has been shown that EVs derived from different glial cells participate in processes associated with neuroinflammation (astrocyte-derived EVs) and common neurodegenerative diseases such as Alzheimer's disease (Microglia-derived EVs) (Zalevsky, A. O., & Lomakin, Y. A. et al. 2022).

Additionally, the role of EVs in the events underlying sepsis (Levy, J. H. et al. 2022), renal and liver diseases (Karpman, D. et al. 2019; Nakagawa, H. et al. 2022), post-transplant complications (Bruno, B. et al. 2020) hematologic and metabolic disorders (Barbieri, S. S. et al. 2019; Mirmira, R. G. et al. 2022) was demonstrated.

# 1.5 Potential applications and challenges in the field

As it was previously mentioned, EVs present different molecules on their surface and internal composition which derive from the donor cell, and then, through the so-called "horizontal transfer", they are uptaken by the recipient cell generating phenotypical changes. All this process contributes to the vital clinical applications of EVs, such as biological markers for diagnosing diseases or monitoring treatments, delivery vehicles for drugs, and therapeutic vectors.

The importance of the presence of a specific pattern of proteins and nucleic acids in the composition of the EVs, not only lies in the fact that this composition depends on its cell of origin and its state (physiological basal-activated or pathological) but also, is like a signature and allows them to be tracked (Nazarenko 2020; Yáñez-Mó et al. 2015; Nazarenko et al. 2010; Simons und Raposo 2009;). It is widely known that early detection of many diseases has a crucial repercussion on their prognosis and in this matter, this functional property of EVs has critical importance, since the fact of being able to track EVs through its cargo, as coming from tumor cells or activated immune cells, would allow the diagnosis and prognosis of diseases through early and minimally invasive studies, such as liquid biopsy (Nazarenko 2020).

In a study on mutation screening in patients with non-small cell lung cancer (NSCLC), it was shown that exosomes are more sensitive and specific for this purpose than cell-free DNA (Lyden, D. et al. 2014; Ghasemnejad, T. et al. 2021). Similar results were obtained in a study on pancreatic cancer, which showed that a higher proportion of patients in the early stages of the disease had more detectable mutations of the Kirsten rat sarcoma viral oncogene homolog (KRAS) in exosomal DNA than in cell-free DNA (Bernard V, et al. 2017)

In addition to their extensive study as biomarkers in cancer, several studies have focused on EVs derived from different cell types and their cargo, in the diagnosis of various diseases. For example, it was shown that there is a significant decrease in the expression of exosomal miR-193b-3p (a tumor-suppressor miRNA) in the plasma of patients with osteoarthritis compared to healthy participants, thus raising miR-193b in exosomal plasma as a potential biomarker (Lin, K. et al. 2023). Similarly, it has been shown that the composition of hepatocyte-derived or adipose tissue-derived EVs can be used to identify the degree and type of liver disease (Nakagawa, H. et al. 2022).

Regarding the therapeutic applications of EVs, the use of EVs as delivery of nucleic acids or pharmacological drugs, has several advantages, due to their excellent biodistribution and biocompatibility. On the one hand, they are permeable to the membrane and it has also been shown that they can cross the blood-brain barrier (Bai, S. et al. 2015). On the other hand, exosomes derived from normal cells are well tolerated and have low immunogenicity (Nagrath, D. et al. 2016). All this together makes EVs a superior option, overcoming the limitations observed with nanoparticles (T.-T. Tang and B.-C. Liu 2019).

The transport of nucleic acids in EVs makes them stable in circulation and protects them from degradation. The transfer of nucleic acids horizontally by EVs was first described in 2010 when it was shown that THP-1 cells previously transfected with a miR-150 mimic were capable of secreting miR-150-enriched EVs and could be functionally delivered. to recipient cells (Zhang et al. 2010). It has also been shown that, with negligible immunogenicity and toxicity, the administration of exosomes derived from human plasma and loaded with siRNA (small interfering RNA) was able to selectively silence the MAPK1 gene in monocytes and lymphocytes (Wahlgren et al. 2012).

Regarding protein transport, important therapeutic implications have also been shown. In Parkinson's disease (PD), exosomes loaded with the antioxidant protein catalase have been reported to successfully deliver across the blood-brain barrier and provide significant neuroprotective effects in vivo and in vitro PD models (Haney, M.J. et al. 2015). Previously, in 2013, a decrease in schwannoma tumor growth was also reported in an orthotopic mouse model, after performing treatment with EVs derived from the transfected HEK-293T cell line, expressing high levels of the suicide gene mRNA and cytosine deaminase protein. fused to uracil phosphoribosyltransferase (Mizrak et al. 2013).

Beyond the delivery of proteins and genetic material for therapeutic purposes, the administration of drugs using EVs as delivery vehicles has had extensive research (T.-T. Tang and B.-C. Liu 2019). Furthermore, some studies show not only that this is possible, but also that exosome-mediated drug delivery also improved drug stability, biodistribution, and even therapeutic efficacy (Sun et al. 2010; Aqil et al. 2016).

Last but not least, the clinical application of EVs directly as therapeutic targets was also studied. It is known that EVs are involved in a hundred pathological processes, and are even secreted in greater quantities in said processes, so reducing the level of EVs or inhibiting EV uptake into target cells could be an excellent therapeutic option (T .-T. Tang and B.-C. Liu 2019). This could be possible by certain substances and antibodies (Mulcahy et al. 2014), however, EVs production, release, and uptake are meticulously regulated processes and more knowledge is required for their manipulation.

The numerous advantages of using EVs as tools for diagnosis and treatment are, at this point, unquestionable. As already stated, the use of EVs as biological markers would allow early and minimally invasive diagnosis of many diseases, improving the prognosis for millions of patients. In turn, as therapeutic agents, their small size facilitates their extravasation, translocation through physical barriers, and passage through the extracellular matrix and their natural composition of lipids and surface proteins allows them to evade phagocytosis, prolong the half-life in blood and reduce long-term safety concerns. In addition, the transport of therapeutic agents (whether drugs, proteins, or genetic material) through encapsulation within EVs improves stability and bioavailability at the site of action.

However, there are still many challenges in this field. First, there are still many processes underlying the biology of EVs that are poorly understood, such as their mechanism of production and uptake. Concerning therapeutic applications, large-scale and efficient production of sufficient quantities of EVs with therapeutic payloads for clinical trials under Good Manufacturing Practice (GMP) standards would be necessary. On the other hand, its great heterogeneity in terms of size, concentration, and composition, associated with its small size and low refractive index, provides unique challenges when establishing standardized protocols regarding its isolation and characterization methods. For example, even though EVs come from the same cell types, they may have conflicting effects as a consequence of differences in cell culture conditions and differences in purification protocols used or due to the current lack of robust characterization of the EVs. extracellular vesicles.

# 2. Nanoparticle Tracking Analysis

NTA is a characterization method, useful for rapid assessment of the size and concentration of EVs (Øvstebø, R. et al. 2017; Nieuwland, R. et al. 2014; Wang, L. et al. 2020; Nieuwland, R et al. 2018; Pogge von Strandmann, E. et al. 2019; Verdier, M. et al. 2022). During a measurement, suspended particles are illuminated by a laser beam, and the light scattered by each individual particle in the field of view is focused by the microscope onto the image sensor of the video camera which records the particle movement. The NTA software then identifies and traces the random thermal movement of each particle (Brownian movement) to determine

the diffusion coefficient, which is used together with the temperature and viscosity of the suspended liquid to calculate the particle size, through the Stokes-Einstein Equation.

The method of choice for the rapid characterization of nanometer-range particles in suspension, for many years, has been dynamic light scattering (DLS). In comparison, NTA presents as advantages not only that it considers individual particles measurement providing a higher resolution for multimodal samples, but also that it allows evidence of aggregation phenomena through direct visualization in the video recorded. In recent years, NTA has become an essential tool within the EVs research field. Although this technique has been evaluated to study two-dimensional diffusion in membranes since the early 1990s (Qian, H. et al. 1991), its application to the measurement of EVs is even more recent, being reported for the first time in 2011 (Sargent, I. L. et al 2011).

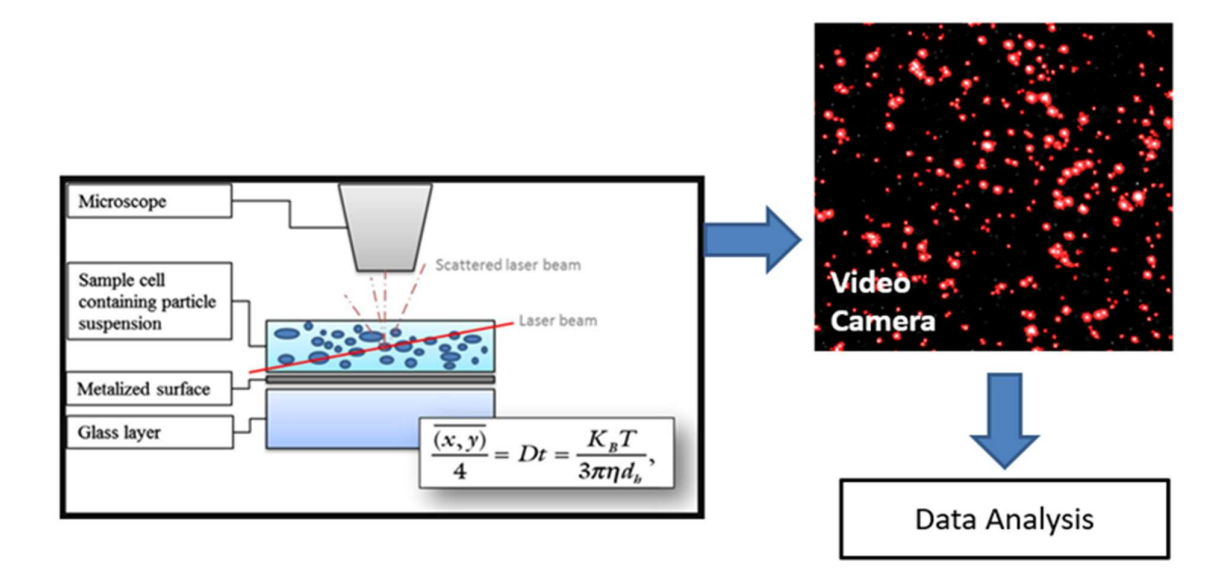


Figure 4: Principle of NTA measurements and Stokes–Einstein equation. Image adapted from Garidel, P. et al. 2016.

Nowadays, NTA instruments are widely used to estimate the size and concentration of nanoparticles, and are also capable of phenotyping when combined with affinity-linked fluorescence, since they can operate in 2 modes: fluorescent and scatter mode (Fig.5). The difference is that scatter mode, all particles whose scattered light exceeds the detection threshold intensity will be measured, regardless of whether the particle is fluorescently labeled or not. In contrast, in fluorescent mode, scattered light is blocked by a filter, and only fluorescently labeled particles will be detected and measured. This characteristic, through the labeling of specific membrane proteins, allows NTA to carry out two crucial tasks for the characterization of EVs in biological samples: the differentiation of EVs from non-EV

nanoparticles and the specific detection for quantification of EVs from different cell subpopulations.

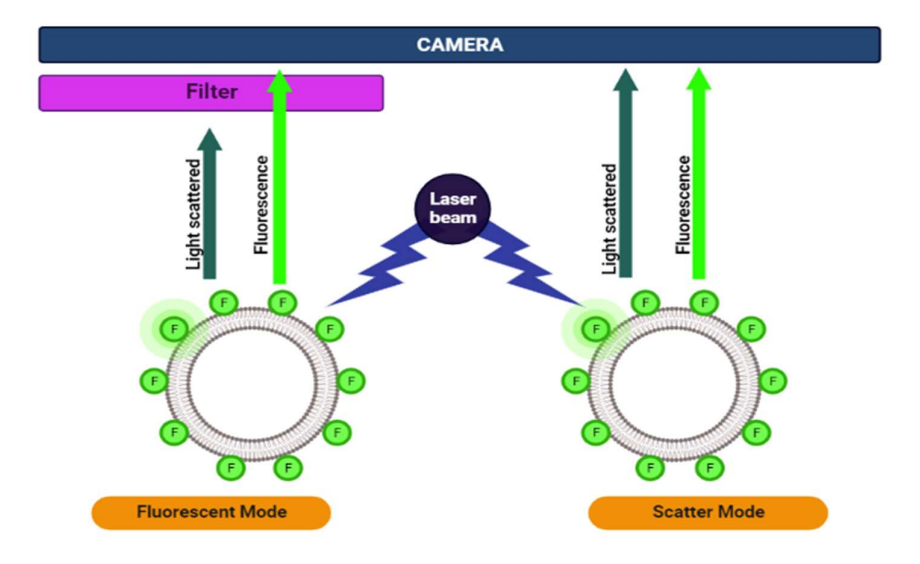


Figure 5.NTA scattering and fluorescent modes. Image created with BioRender.com

The results of the measurements can be affected by inaccurate temperature, incorrect evaluation of viscosity, external vibration, intensity and wavelength of the illumination, collection angles of the objective, sensitivity of the camera with the applied settings, the brightness of the scattering particles (which depends on the particle size and refractive index), the duration of the measurements, the analysis software and the operator profile (Sargent, I. L. et al. 2013). The NTA instrument was created to measure homogeneous artificial, with high refractive index nano-objects and is facing now the challenge of measuring biological, heterogeneous, with low refractive index nanoparticles. Because of its relatively recent development, it has not yet achieved the desired standardization, which is necessary for any analytical method (Nazarenko, I. et al. 2020; Sargent, I. L. et al. 2013).

# 3. Reference materials in the EVs research field

Last but not least, in order to achieve standardization of EVs characterization, it is necessary not only to use written standards and reference methods but also "reference materials", which were defined as "any material that assists in the evaluation of the reproducibility of a measurement" (Welsh, J. A. et al. 2020). An important concept that emerges from this definition is that in order to ensure the choice of a suitable reference material, three things must be taken into account: the principle/mechanism of action of the study method to be used, how the results obtained through this method could be altered and the characteristics/properties of the sample to be evaluated. Considering this, when choosing a suitable reference material for the

calibration of NTA instruments for the measurement of EVs, it should be taken into account that NTA is an optical method, that the result depends both on the set parameters and the detection threshold in the instrument (sensitivity, resolution, minimum brightness, etc.), as well as the physicochemical properties of the sample to be evaluated, and therefore the reference material must have similar properties to the EVs. Keeping in mind that EVs are undetectable by standard means of light microscopy due to their small size and low refractive index, finding the proper reference material represents a real challenge.

Determining that a reference material can be used in optical techniques for the validation of size distributions using light scattering requires knowledge of the refractive index. The refractive index is a measure of how well light travels through a material. The higher the refractive index, the slower the light travels, causing a correspondingly larger change in the direction of light within the material. This property is crucial in optical techniques, which are routinely used to measure and count extracellular vesicles, such as NTA. A more detailed discussion of the refractive index is beyond the scope of this work but has been reported elsewhere (Varga, Z. et al. 2018; Van Der Pol, E. et al. 2014; Gardiner, C. et al. 2014).

The concentration of EVs is reported in most of the publications in this field, however, it is one of the most difficult parameters to obtain accurately. For example, the sensitivity limit for the different techniques used is generally not reported, even though this limit is crucial to know how many of the smallest and most abundant EVs are detected. Accurate measurement of the concentration of a sample requires the detection of all particles and although this is not currently possible, it could be improved by reporting sensitivity limits with reference materials and detectable events within a given detection window (Welsh, J. A. et al. 2020).

To date, most of the studies that have attempted to standardize an NTA protocol for EVs measurements, have been carried out using polystyrene microspheres as reference material. However, it is known that polystyrene particles have a higher refractive index than reported for EVs, scattering approximately 4 times more light than vesicles of the same size, resulting in an underestimation of EVs concentration (Gardiner, C. et al. 2013).

Silicium dioxide, also known as silica, is an oxide of silicium with the chemical formula SiO2, most commonly found in nature as quartz and in various living organisms. It has been shown that SiO2 nanoparticles present a refractive index closer to that of EVs and therefore could represent a more appropriate reference material for the calibration of optical methods for the measurement of EVs (Varga, Z. et al. 2018).

# **AIM OF THIS PROJECT**

The main aim of this project is to evaluate the performance of NTA as a characterizing method for the measurement of EVs, providing robust and reproducible data.

The motivation for this work is triggered by the fact that all potential clinical applications of EVs are limited by the lack of standardization in their characterization methods. It is known that due to their small size, low refractive index, and polydispersity, this task presents unique challenges.

To achieve this aim, my specific objectives can be divided accordingly with the modes of the instrument:

# Measurement of reference material and EVs using NTA in scatter mode

- I. To evaluate NTA performance when measuring synthetic reference materials:
- Establish the standard operating procedures (SOPs) for the measurement of homogeneous reference material of determined size and concentration, using NTA in scatter mode, trying to obtain a concentration correction factor close to 1 (being the correction factor the relation between the "expected concentration" and the "concentration measured").
- 2) Evaluate the performance of the different SOPs for **heterogeneous reference material**, by using them for measurement of SiO2 nanoparticles of different sizes (known size and concentration).
- II. To test the applicability of the established SOPs for the measurement of EVs.

# Measurement of reference material and EVs using NTA in fluorescent mode

I. To establish SOPs in the fluorescent mode for the measurement of homogeneous reference material, calculate the relative correction factor and use the established SOPs in the fluorescent mode for the measurement of synthetic EVs of different diameter ranges and different fluorophores molar ratios.

# **MATERIALS AND METHODS**

# **Materials**

# 1. Reference material, synthetic vesicles and cell lines.

#### 1.1 Reference Material.

SiO<sub>2</sub> nanoparticles of different diameters were provided by micromod Partikeltechnologie GmbH (Germany), through Particle Metrix (Germany). An expected concentration (Table 1) and an established set of standard operating procedures (SOPs, data not shown) for each size of SiO<sub>2</sub> nanoparticles were given by the provider.

Table 1. SiO2 nanoparticles: size and stock concentration.

Size	30 nm	50 nm	70 nm	100 nm	150 nm	200 nm	300 nm	400 nm	500 nm
Expected concentration	8.9 E14	1.9E14	7 E13	4.8E13	1.4E13	6E12	1.8 E12	7.5E11	3.8E12
Polydispersity index	<0.2	<0.2	<0.2	<0.2	<0.2	<0.2	<0.2	<0.2	<0.2
Porosity	No pores								

The size of the particles, according to supplier specifications, was determined by dynamic light scattering, up to 1000 nm, and using a Coulter Counter for particles larger than 1000 nm. The number of particles per mL or mg (concentration) was calculated based on the density and the nominal size (100 nm, etc.)

#### 1.2 Cell line.

Table 3. Cell line and culture conditions.

Cell line	Description	Growing cell culture conditions	3D culture conditions
HT1080	Parental fibrosarcoma cell line (ATCC cell culture collection)	RPMI 1640 + 10% FBS	3D CoSeedis™ (abc biopapply, Switzerland)

# 1.3 Synthetic Extracellular Vesicles (SEVs).

A total of nine samples were provided by Max Planck Institute for Medical research Heidelberg (in collaboration with Prof. Dr. Oskar Staufer, Kennedy Institute of Rheumatology, University of Oxford), in 3 different size ranges and different fluorophores molar ratio.

Table 2. Synthetic Vesicles.

Synthetic Vesicles Characteristics (MPI Heidelberg)				
Diameter	Concentration	Molar ratio f	luorphores (%)	Fluorphores density
(nm)	(Vesicles/ml)	Rhodamine B	Atto488	(fluorphores/nm)
89	7,10E+12	0	0	0
93	7,20E+12	0,1	0,1	0,002
88	7,10E+12	1	1	0,02
167	2,00E+12	0	0	0
182	2,10E+12	0,1	0,1	0,002
170	2,20E+12	1	1	0,02
633	1,20E+11	0	0	0
612	1,25E+11	0,1	0,1	0,002
624	1,10E+11	1	1	0,02

# 2. Media and supplements

Table 4. Media and supplements.

Product	Company
RPMI 1640	Gibco, Life technologies, Darmstadt, Germany
Fetal bovine serum	PAN Biotech, Aidenbach, Germany
PBS	Gibco, Life technologies, Darmstadt, Germany

# 3. Chemicals and reagents

Table 5. Chemicals and reagents

Product	Source
1x Phosphate Buffered Saline (PBS)	Molecular biology department, Uniklinik, University of Freiburg
0,1x Phosphate Buffered Saline (PBS)	Molecular biology department, Uniklinik, University of Freiburg
NaOH 0.5M	Carl Roth, Germany
Sodium Azide 0,05%	Sigma Aldrich, Germany
Glutaraldehyde 1%	Department Exosome and Tumor biology, Uniklinik, University of Freiburg
Uranyl acetate 1%	Department Exosome and Tumor biology, Uniklinik, University of Freiburg
1x HEPES buffer	Biochrom AG, Department Exosome and Tumor biology, Uniklinik, University of Freiburg
Ethanol 70%	Liquid Production, Germany
ddH2O Stakpure (0.2µm filter)	Uniklinik, University of Freiburg
Dimethyl sulfoxide (DMSO)	Sigma-Aldrich Chemie GmbH, Germany
EDTA	Carl Roth, Karlsruhe, Germany
GeneRuler 50 bp DNA Ladder	Thermo Fisher Scientific, Germany
TrypanBlue (0.4%)	Sigma-Aldrich, Germany
Trypsin (2.5%)	Gibco, Life technologies, Germany
SDS-PAGE running buffer (10X)	250 mM Tris base, 2.5 M Glycine, 1% SDS, adjusted to pH 8.3

# 4. Kits and instruments

Table 6. Kits and instruments

Product name	Company	Purpose
Zeta View TWIN – Nanoparticle tracking		NTA SOPs establishment. Sizing, quantification and fenotipification
TFF-MV	HansaBioMed Life Sciences, Estonia	
Proteus X-Spinner 2.5, 100kDa	SERVA Electrophoresis GmbH, Germany	
Amicon Ultra-15 Centrifugal Filter Units, 10 kDa	Merck Millipore, USA	EVs isolation from cell culture
Automatic Fraction Collector	IZON, New Zealand	
qEVoriginal / 35 nm Gen 2 Column	IZON, New Zealand	
Micro BCA Protein Assay Kit	Thermo Fisher Scientific, USA	Protein detection
Plate Reader Infinite M Plex	TECAN, Switzerland	
e-MycoTM Mycoplasma PCR detection kit	LiliF Diagnostics, iNtRON biotechnology, Korea	Test to potential Mycoplasma contamination
Talos L120C G2 Transmission Electron Microscope	Thermo Fisher Scientific, USA	Direct visualization

# 5. Consumables

Table 7. Consumables

Product	Source		
Falcon tubes (15 mL)	Corning Brand, Mexico		
Polypropylene conical falcon tube (50 mL)	Corning Brand, Mexico		
Syringe (20mL)	Braun, Germany		
Pore filters millex (0.22µm)	Merck Millipore Ltd, Ireland		
Disposable serological pipettes	Cellstar,USA		
Serva proteus X-spinner 100kDa Ultra-filtration Tube	ProteinArk, Germany		
Eppendorf tubes (0.5mL, 1.5mL, 2 mL)	Alpha Laboratory, UK		
Micropipete plastic tips (200µL)	Brand, Germany		
Micropipete plastic tips (1000μL)	Brand, Germany		
Sterile insulin syringes (1mL), Omnifix 100 solo	BRAUN, Germany		
Plastic microplates (96 wells)	Greiner bio-one, Germany		
Parafilm Bermis Sigma Aldrich,	USA		
Nitrite powder free examination gloves	MicroTouch Nitra-Tex, China		
Glass flasks	Schott, Germany		
Copper grids for TEM	Department Exosome and Tumor biology, Uniklinik, University of Freiburg		

# **Methods**

# Nanoparticle tracking analysis.

As it was previously explained, NTA is an optical method for measuring nanoparticles in suspension in a range from 10 - 1000 nm based on the analysis of Brownian motion. The particles in the sample are illuminated with a laser beam, and the scattered light is focused by a microscope onto a camera which records the particle movement. Then, the random thermal motion of each particle is tracked by the NTA software to calculate size and concentration.

There are two modes on NTA ZetaView® instruments: "scatter mode" and "fluorescent mode". In scatter mode, all particles above the detection threshold will be counted, regardless of whether they are fluorescently labeled or not. In fluorescent mode, scattered light (the same wavelength as the laser) is blocked and only particles that emit fluorescence are detected. Light scattered by unlabeled particles cannot reach the camera (Fig.5). Another difference between scattering and fluorescent mode is regarding the influence of the size of the particle evaluated on the measurement result. In the former, the concentration measurement is affected by the size of the particles, while the latter is not dependent on the size, but on the fluorescence intensity.

The experiments in this work are performed by the nanoparticle tracking analyzer: ZetaView® instrument (Particle Metrix, Germany) model PMX-220 (TWIN), equipped with the camera: FpSec 90. Analysis is made by Software ZetaView (version 8.05.14 SP7).

# 1. Measurement of reference material and EVs using NTA in scatter mode

Prior to starting, samples were diluted ddH2O (0.2µm filter, Uniklinik, University of Freiburg) and then introduced in the instrument without bubbles. The final dilution is determined by the number of detected particles, which should be between 50 and 200. Beyond that range, both size and concentration determination may be incorrect.

Measurements were made by running the video acquisition, setting the parameters for the SOP that is going to be used, and the folder where the files are going to be downloaded. The system was rinsed between the different measurements.

The parameters included in the SOPs settings can be divided in two groups: pre and post - acquisition parameters. The former are those taken into account for the video recording, while the latter are digital filters applied to the images. Some of these parameters were kept constant in all the measurements, regardless of the SOP or the particle used as we can see in table 8.

Table 8. NTA Instrument settings.

Parameters that were kept constant in all measurements (regardless of particle size or SOP used)	Modified parameters during measurements for optimization/generation of SOPs.
<ul> <li>Temperature: 25°C</li> <li>Positions: 11</li> <li>Cycles: 1</li> <li>Resolution: highest</li> <li>Tracking radius: 100</li> <li>Size classes log: 64</li> <li>Laser: 488nm.</li> </ul>	<ul> <li>Sensitivity</li> <li>Shutter</li> <li>Frame rate</li> <li>Minimum brightness</li> <li>Minimum area</li> <li>Trace length</li> </ul>

Brief description of the parameters modified between the different SOPs:

**Sensitivity:** Ability to detect a signal. It has a direct influence on the count of detected particles and must be adjusted considering the light scattered from the particles in the sample and their refractive index, which means that very small particles and those with a low refractive index require a higher sensitivity setting than large and/or high refractive index particles.

**Shutter:** Adjust the length of the camera's exposure time. The indicated value is reciprocal in seconds, therefore, high values represent a short exposure time and low values represent longer exposure times. The number of detected particles and the scattering intensity are inversely related to the shutter value.

**Frame rate:** Considering that the instrument captures a video for a size measurement, it is easy to understand that a certain number of images are necessary, to later analyze them and determine the diffusion coefficient of each individual particle. The frame rate indicates the number of recorded frames per time period (frames per second).

**Minimum Brightness:** Defines the threshold at which a gray value is recognized as a white pixel, where all the information for subsequent analysis is taken into account. In the background of the image, the pixel will be black since the gray value is less than the threshold. Default values for biological particles such as extracellular vesicles range from 20 to 30.

**Minimum area:** Represents the minimum number of pixels that a particle contains to be analyzed in the statistics.

**Tracelength:** his parameter defines how many consecutive video frames a particle must be traced to be included in the final analysis and statistics. As a general rule, the resolution of the particle size distribution improves as the trace length increases.

The analysis was performed by the NTA software, removing all the camera positions considered outliers. The reasons why the instrument might remove them are explained in table 9. Measurements that presented more than three positions removed for analysis were excluded by consensus with the research team. Measurements that presented results extremely far from the mean were also considered atypical values, by probable alterations in the dilutions made, and were also excluded.

Table 9. Reasons for position removal.

Outlier message	Meaning	Possible reason for removal
1. Min traces	A particle must be followed for at least 5 or more traces.	Too few particles; concentration too low
2. Max drift	Flagged when the speed of the particles exceeds 30µm/sec	Temperature issues; Buffers of different viscosity or salt content were mixed; Leakage or bubbles in the fluidic system
3. Range size	Flagged when particles are detected that are lower than 10nm and larger than 3000 nm.	Detected particles are too large or too small for reliable size determination
4. Range number	Flagged when the average number of particles is lower than 10 and larger than 800.	Too few or too many particles in the sample
5. GRUBBS Number	Deviation of the average number of particles is too large compared to other positions	Heterogeneous distribution of particles throughout the cell
6. GRUBBS MI	Deviation of the mean intensity of the particles is too large compared to other positions	Air bubble; large particles; High scattering contaminations in the sample; Background from free fluorescence dye or protein monomers;
7. GRUBBS Size	Deviation of the size of the particles is too large compared to other positions	Heterogeneous distribution of large particles throughout the cell

# 1.1 SOPs establishment for measurement of SiO2 nanoparticles of determined sizes.

Repeated measurements of dilutions of beads of known concentration and size were made to assess whether the measured concentration is the same as the expected concentration.

To calculate the relationship between the "expected concentration" and the "measured concentration" during the experiments, the concentration correction factor shown in the following formula was used:

$$Concentration Correction Factor = \frac{Concentration Expected (stock concentration)}{Concentration measured}$$

In order to obtain correction factors close to 1 (which means that the measured concentration is similar to the expected one), separate measurements were made by SiO2 nanoparticle size, with different parameters set in the instrument, in order to establish a series of Standard Operating Procedures (SOPs) that are capable of measuring size and concentration with adequate precision.

# 1.2 Calculation of the correction factor for each SOP established

Once the SOPs corresponding to each size had been established, the parameters in the instrument were not changed anymore. Measurements were made with the established SOPs (minimum of 10 measurements for SiO2 nanoparticles of the ideal size range) with two objectives:

- Establish the concentration correction factor corresponding to each SOP that will then be set in the instrument, together with the rest of the parameters, for future measurements.
- Verify that the concentration correction factor obtained is valid in several different measurements for the ideal size range, maintaining a linear relationship between the expected and measured concentration.

In order to calculate the correction factor corresponding to each SOP, experiments were carried out as follows:

- A minimum of 10 measurements were made for SiO2 nanoparticles of 100, 200, 300, 400 and 500 nm, using the corresponding SOP for each size.
- In each measurement made, the relationship between the expected concentration and the obtained one was calculated.
- Finally, the average of all the results obtained determined the value of the correction factor for each SOP respectively.

# 1.3 SOPs cross-compatibility and resolution evaluation

We defined the "SOP cross-compatibility" as the performance of the different SOPs when used for the measurement of SiO2 nanoparticles outside the ideal size range. To evaluate this, each SOP, with the correction factor set in the machine, was used for the measurement of SiO2 nanoparticles of different sizes, including the ideal size range. At this point, the relation between the concentration that we expect and the one that we obtain was calculated as: "error precision factor" and it is a parameter to estimate the compatibility of each SOP with the measurement of different sizes of particles, and how far (or close) are the obtained results from the expected ones.

Considering the resolution as the ability to distinguish two different signals as independent to each other, we did 10 measurements of 100 and 200 nm SiO2 nanoparticles in a 1:1 ratio of mixture to evaluate the SOP resolution to discriminate between particles of different sizes in a mix.

# 1.4 EVs measurement using the established SOPs

In order to evaluate the performance of the established SOPs to perform EV measurements, two experiments were carried out:

- Sizing and quantification of synthetic EVs, with a given concentration and size. Nine samples of synthetic EVs were provided by the supplier, divided into three different size ranges (88-93-89 nm, 167-182-170 nm and 633-612-624 nm). The measurement of each sample was carried out, using the SOPs considering the size range as shown in table n°10.
- Sizing and quantification of EVs derived from cell culture, with unknown concentration and size. EVs were isolated by SEC and TFF from cell culture of the HT1080 parental cell line under 3D conditions. All the samples obtained were measured with NTA using the SOPs established for SiO2 nanoparticles of 100 and 500 nm.

Table 10. SOP used for synthetic EVs measurement according to their size.

Synthetic EVs size range	SOP used for measurements in scatter mode
88-93-89 nm	SOPs established for 100 nm SiO2 nanoparticles

# 1. 5 Measurement of SiO2 nanoparticles of 30, 50, 70, and 150 nm diameter using the established SOPs.

The objective of this step was to test the applicability of the SOPs established for SiO2 nanoparticles of 100, 200, 300, 400, and 500 nm, for the measurement of smaller particles in order to determine the precise range of detection of each SOP. In these experiments, the SOPs were used for the measurement of SiO2 nanoparticles of 30, 50, 70, and 150 nm diameter in at least 10 measurements for each combination possible.

# 2. Measurement of reference material and EVs using NTA in fluorescent mode

# 2.1 Establishment of the SOP in fluorescent mode.

Standard fluorescent NTA (100 nm fluorescent green polystyrene particles) was measured in a minimum of 10 measurements, using different instrument parameters, until a set of settings was achieved that measured the fluorescent particles with adequate precision.

# 2.2 Relative correction factor calculation

To calibrate the instrument in fluorescent mode to make concentration measurement possible, the relative concentration correction factor was calculated.

For this, the measurements were made with the new SOP for fluorescent mode (previously established) and then they were compared with measurements made with the SOPs established according to the size of the particles in scatter mode. The experiments to calculate the relative correction factor were carried out as explained below:

- A first dilution of 1:1000 was made and then a new dilution of 1:1000 in a final volume of 2ml. Final dilution: 1:1000000.
- The diluted sample was entered into the instrument using a 1ml syringe, without bubbles.
- Once the sample was introduced, the video acquisition was run twice: First, using the SOP previously established for the fluorescent mode and then, using the SOP established in scatter mode according to the size of the particle (in this case, for particles 100 nm, since the fluorescent standard used is 100 nm fluorescent green polystyrene particles).
- The same procedure was repeated 13 times, each time obtaining a different concentration in fluorescent mode and in scatter mode, and the product of the relationship between them was calculated.
- Finally, the average of the results obtained from said relationship for each of the measurements was calculated, the result of which was the relative correction factor for the SOP in established fluorescent mode.

# 2.3 Measurement of synthetic vesicles of different sizes and fluorophores densities.

The SOP established for fluorescent mode, with the relative correction factor set between its parameters, was used for the measurement of synthetic EVs with different molar ratios of fluorophores. At each opportunity, the synthetic EVs were also measured using the SOP established in scatter mode, according to their size.

# Cell culture

# 1. Storage and revival of cells.

HT1080 parental cells were taken from liquid nitrogen stock (Institute for Infection Prevention and Hospital Epidemiology – Research Group: Exosomes and Tumor Biology). For revival, frozen cells were placed in a water bath (37 °C) under constant supervision until thawed and then placed immediately into a cell culture T75 flask filled with 20 mL of pre-warmed (37 °C) 10% FBS-complete media. Cells were incubated at 37°C and 5% CO2 for 24 h. Previously, by gentle horizontal shaking of the cell culture flask, even distribution was ensured. The next day, the medium was removed and replaced with a fresh prewarmed complete medium (RPMI 1640 media [+] L-Glutamine (Gibco Life Technologies, Germany) supplemented with 10% FBS).

For storing, the cells were washed once with 1x PBS and trypsinized with Trypsin-EDTA

mixture (0.05 % Trypsin, 1 mM EDTA in 1x PBS). The detachment of the cells was supervised under the microscope, followed by the addition of 8 mL of complete media to stop the enzymatic effects of trypsin.

The suspension of cells was centrifuged by centrifugation at 800 g for 5 minutes, and further diluted in freezing media (Cell culture media supplemented with 20% of FBS and 10% DMSO). A total of 1-2 million cells were aliquoted in each cryotube and stored in a Nalgene® Mr. Frosty freezing container at -80 °C that provides a cooling rate of 1 °C/min required for the successful cryopreservation of the cells.

# 1.1 Trypan blue

The cells were detached as indicated above (see storage and revival of cells), and a volume of 10  $\mu$ L was mixed with 1:1 volumes of Trypan Blue solution 0.4 % (Sigma-Aldrich, Germany). 20  $\mu$ L of the mixture was introduced in a Luna<sup>TM</sup> Counter slide for counting, and determination of the percentage of viable and dead cells, in a Luna <sup>TM</sup> Automated cell counter (Logos Biosystems, SK).

# 1.2 Mycoplasma test

All cell stocks were tested for possible mycoplasma contamination, before being permanently stored in the liquid nitrogen tank. As it was explained before, cells were counted and the percentage of viability was checked, from a cell suspension after trypsinization. A volume corresponding to 5xE4 cells was placed in a 1.5 mL microcentrifuge tube (Eppendorf®, Germany) filled to 1 mL with fresh complete medium. The tube was spun at full speed for 15 seconds, the supernatant discarded, and the pellet resuspended in 1x PBS, followed by another 15 second spin. Finally, the pellet was resuspended in 100 µL of 1x PBS and stored at -20 oC. Mycoplasma testing was performed with the e-Myco™ Mycoplasma PCR Detection Kit (LiliF Diagnostics, Korea) following the manufacturer's instructions.

#### 2. Culture of cells in 3D

Cell culture in 3D conditions was performed using 3D CoSeedis™ (abc biopapply, Switzerland). This culture system is a scaffold-free co-culture system, consisting of a matrix with 100 microwells/cm² made of 2.4% agarose gel in H₂O. Two-dimensional (2D) culture is currently used as the "gold standard" for the study of ex-vivo cell communications, among other reasons because it is simple and easily accessible. However, the culture environment cannot represent the extracellular matrix (ECM) microenvironment in vivo. Three-dimensional (3D) cellular systems allow an efficient EV production under controlled conditions and mimicking the in vivo physiological environment for producing in vivo like EVs. Unlike the 2D culture system, in which cell-to-cell interaction is only along the edge, 3D cell culture involves cell stretching and

interactions from all angles, as well as cell-to-ECM interactions, which in turn, promotes cell signal transduction and proliferation

To perform the 3D cell culture, 3D CoSeedis™ matrices were first equilibrated by immersion in 3 mL of serum-free media for 3-12h in the incubator. The number of cells was determined as explained before, and the cell suspension was prepared in a concentration of 7·10<sup>4</sup> cells/cm<sup>2</sup> (= cells/mL) in media supplemented with 2.5% of EV-depleted serum and then added to each matrix in a 6-wells plate, and allowed to grow in the incubator for 24h.

For EVs production, after 24hs, 3D CoSeedis<sup>™</sup> matrices were transferred to a new 6-well plate and allowed to grow in the incubator for 7 days with daily-check monitoring of cell viability and growth under the microscope.

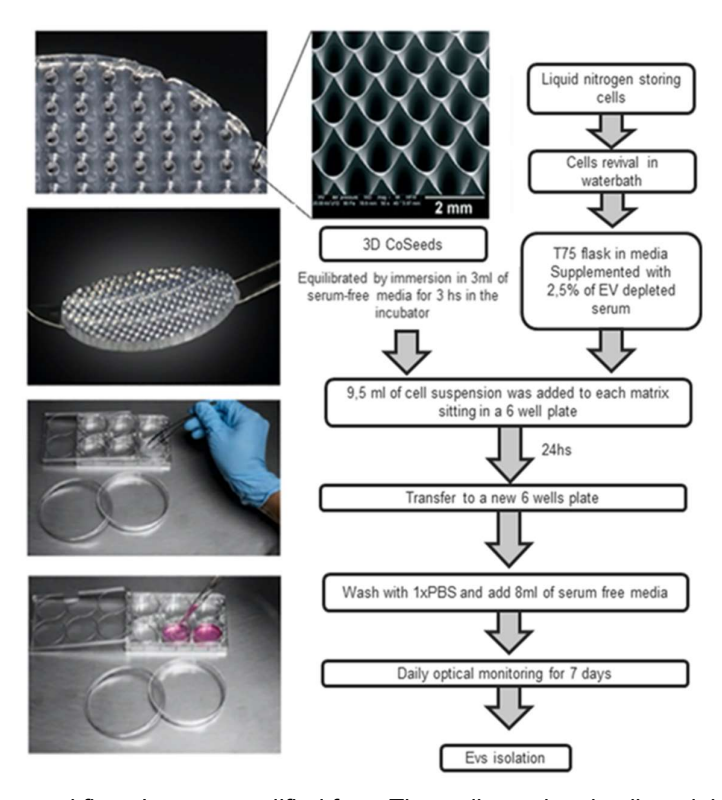


Figure 6. Cell culture workflow. Images modified from Three-dimensional cell models for extracellular vesicles production, isolation, and characterization (Paniushkina et al., 2020).

On the 7th day, conditioned cell culture media was collected for exosome isolation. First, the matrices are lifted out of their culture plate and placed upside down into the new 6 wells plate with PBS. Next, the plate was centrifuged for 1 min, at 300g, 4°C, and then, empty matrices were removed from the wells and harvest cell aggregates were transferred to the tube containing the cell conditioned media. The tubes are centrifuged for 5 min, at 800g, 4°C (twice) to remove cell debris, and the supernatant was collected for exosome isolation.

## 2.1 FBS - EV depleted production

Due to the fact that FBS (Fetal Bovine Serum) can present its own EVs, and with the aim of carrying out a purified evaluation of the EVs derived from cell culture, we proceeded to produce FBS-EV depleted. First, the tubes and the centrifuge rotor were pre-cooled for 24 hours at 4°C. The next day, an aliquot of inactivated FBS was taken (in 50ml Falcon tubes, at -20°C) and the centrifuge tubes were filled, which were centrifuged for 16h overnight at 32000rpms. After ultracentrifugation, the supernatant was taken, living approximately 1 ml of volume in the base of the tube, to avoid taking the pellet anyhow. Finally, FBS was filtered (using 0.22 pore filters) and aliquoted in 15 ml Falcon tubes. Aliquots were kept at -20°C until used. All steps were made under sterile conditions.

### 3. EVs isolation

For EVs isolation, the supernatant collected from the cell culture after centrifugation was centrifuged at 5000 g, 4°C, for 45 min. The supernatant was used to isolate small EVs by size exclusion chromatography (SEC) and the pellet to isolate large EVs by tangential flow filtration (TFF). In the diagram n°2, the isolation workflow is shown.

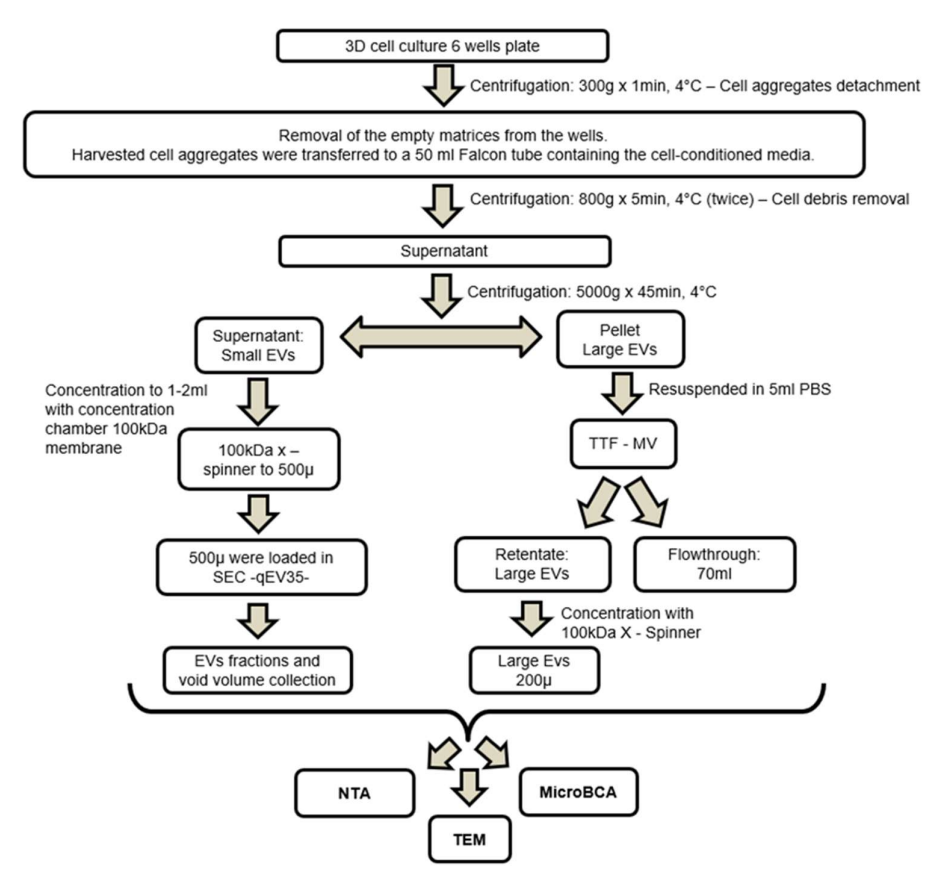


Figure 7. EVs isolation workflow. 3D: tridimentional; EVs: Extracellular vesicles; SEC: Size exclusion chromatography; NTA: Nanoparticle tracking analysis; TEM: Transmission electron microscopy.

All the samples obtained after isolation (from SEC and TFF) were aliquoted for characterization by using the established NTA SOPs for sizing and quantification and micro BCA for the determination of protein content.

# 3.1 Size Exclusion Chromatography

SEC, also known as gel filtration, is a separation method that allows the fractionalization of molecules or particles according to their molecular size. The sample is charged to the top of the SEC column and the particles go through it at different times according to their sizes, by this, the larger molecules (larger than the pore) go through the interspaces of the gel and are eluted first in the void volume, the smaller molecules penetrate in the gel, presenting more retention time and presenting latter in the fractions. In other words, larger molecules elute first, and smaller ones will elute last.

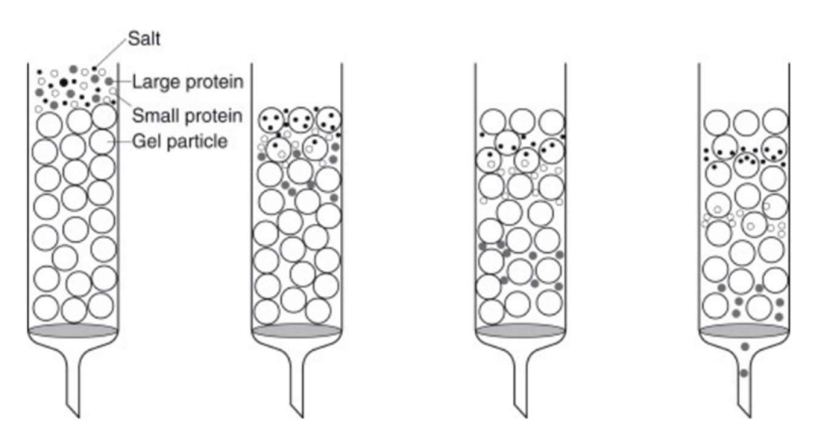


Figure 8. SEC principle scheme: Progressive separation of molecules of different sizes by gel filtration (Image from: Robinson, R. K. (2014). *Encyclopedia of food microbiology*. Academic press).

For performing SEC, the Automatic Fraction Collector (AFC) by IZON science was used. The AFC can collect the resulting fractions from the column by an automatic differentiation between the volume of void (not containing any EVs) and the volume of the fractions containing the EVs. To perform this evaluation, it was used the qEVoriginal 35 column.

For sample preparation the cell culture media supernatant was concentrated to 1-2ml using a concentration chamber 100kDa membrane, and then to 500 $\mu$  using a X-spinner 100kDa ultrafiltration tube.

For the qEVoriginal column preparation, it is equilibrated at room temperature for at least 20 minutes before use, and then rinsed with 30 ml of filtered 1x PBS.

For sample loading and SEC fractions acquirement: the 500µL of concentrated EVs sample was charged into the column (minimal volume needed to perform SEC using qEVoriginal); The column start running and when the void volume is collected, the carousel move through the different positions collecting the specified volume for each individual fraction.

After the fraction collection, the column was emptied and flushed with filtered 1x PBS (15mL). 0.05% sodium azide is added to the column for further storage at 4°C.

## 3.2 Tangential flow filtration

In tTFF, the liquid is not directly on the filter, compared to dead-end filtration methods, but instead flows tangentially past the filter. As molecules pass through the filter, clogging can be avoided, as seen with dead-end filtration, increasing isolation efficiency and preventing particle compression. Particles that are larger than the filter pores remain in the tangentially flowing stream and smaller ones can pass through the pores.

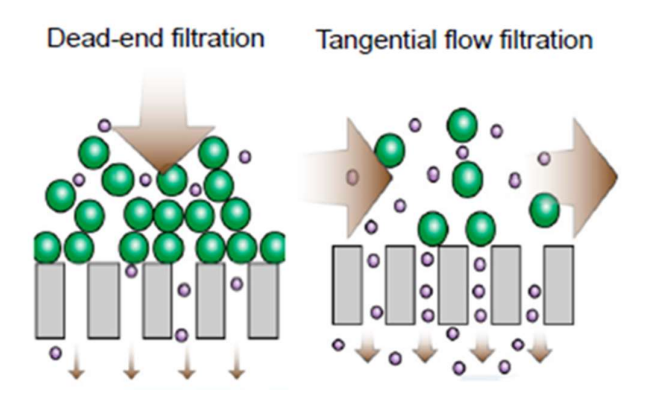


Figure 9: Flow direction differences between dead-end filtration and TFF schematic comparison. For dead-end filtration, the sample flow is vertical to the membrane whereas in TFF is tangential to the membrane (image taken from Busatto et al. (2018)).

For the isolation of EVs by this means, the TFF with a pore size of 200 nm was used, after washing with 10-20ml 40°C MilliQ water.

For sample preparation, the pellet (where the large EVs are assumed to be found after cell culture centrifugation) was re-suspended in 5 ml PBS and filtered through the TFF (filter pore size of 0.8µm). The retentate and the flow-through are both collected. The retained 1-2 ml were concentrated using X-Spinner 100kDa to 200µL and then used for the analysis of large particles.

# **Protein content determination**

### 1. MicroBCA.

In order to analyze the protein contamination in each fraction obtained from the EVs isolation, the protein concentration was measured using the Thermo Scientific Micro BCA Assay Kit according to the manufacturer's instructions. Although the implementation of more than one purification method to eliminate any existing protein contaminants in the sample to be analyzed is recommended in some publications (Brennan et al. 2020), it is also known that there is a risk

of particle loss caused by a step of additional purification.

The assay uses biquinonic acid (BCA) as the detection reagent for Cu+. Cu2+ is reduced to Cu+ by proteins in an alkaline medium and the concentration of Cu+ can be detected in a purple reaction of two BCA molecules with one Cu+. Subsequently, to quantify the amount of protein, the linearity of the absorbance at 562 nm with respect to the protein concentration is used. For analysis, the measured values are exported to Excel, where the standard curve was plotted and used to calculate the protein concentration in each well.

### Assessment of size determination by transmission electron microscopy (TEM)

For qualitative characterization, the size measured with the NTA for silica beads and EVs (synthetic and derived from cell culture), will be confirmed by direct visualization under electron microscopy.

TEM is the most widely used instrument because it has nanometre resolution and can be used to distinguish single extracellular vesicles (EVs) from non-EV particles. In this technique, an electron beam is transmitted through the sample to create a high resolution, nanoscale image. The image is formed from the interaction of the electrons with the sample as the beam is transmitted through the specimen (frequently an ultrathin section, less than 100 nm thick, or a suspension on a grid). Then, the image is magnified and focused onto an imaging device. For sample preparation,  $10~\mu L$  of each sample was dotted onto a copper grid and allowed for absorption for 5 min at room temperature. Then, sample-embedded grids were treated with glutaraldehyde 1% solution, followed by 4 washes with distilled  $H_2O$  (30 seconds each) and then 1% uranyl acetate for 1 minute (for fixation). Due to multiple interferences, the glutaraldehyde step was skipped for the preparation of SiO2 nanoparticle samples. The image

acquisition was performed using the Talos L120C transmission electron microscope (Thermo

Fisher), IMITATE Institute, Electron Microscopy (EM) Core Facility, Ag Walz Innere Med IV, University of Freiburg. And finally, the image analysis was performed using ImageJ (version 1.53t, August 24<sup>th</sup>).

### **RESULTS AND DISCUSSION**

# 1. Measurement of reference material and EVs using NTA in scatter mode

# 1.1 SOPs establishment for measurement of SiO2 nanoparticles of determined sizes.

As previously mentioned, measurements were made for SiO2 nanoparticles of each size with different parameters set in the instrument, until the measured concentration was as close as possible to the expected concentration (given by the provider), without altering the measured size distribution.

The established SOPs, their parameters, and their ideal size range, are shown in the following table:

Table 11. Standard Operating Procedures (SOPs) established

Measurement	Optimized SOP								
Features	SOP100_ExTu	SOP200_ExTu	SOP300_ExTu	SOP400_ExTu	SOP500_ExTu				
Ideal range	100 nm	200nm	300nm	400nm	500nm				
Sensitivity	75	65	60	60	65				
Shutter	100	150	200	300	200				
Frame rate	30	15	15	10	7,5				
Positions	itions 11		11 11		11				
Cycles	1	1	1	1	1				
Resolution	highest	highest	highest	highest	highest				
Min Brightness	20	30	30	40	50				
Min area	10	10	10	20	30				
Max area	1000	1000	1000	1000	1000				
Trace length	15	20	30	50	75				
Tracking radius	100	100	100	100	100				
nm/class (SizeWidthLin)	5 20		20 40		40				
SizeClassesLog	64	64	64	64	64				
Set Temperature	25	25	25	25	25				
Select Laser	488	488	488	488	488				

Table 11. SOPs established. The different SOPs were named, considering the ideal size range to perform the measurement and the name of the research group (ExTu: Exosome and Tumor Biology).

The SOPs established (table 11) were able to calculate with good precision, both the size and the concentration of the SiO2 nanoparticles within the ideal size range.

As it is illustrated in table 11, in most of the cases, our results matched the expectations regarding the different values in the parameters set for each SOP. Firstly, considering the

sensitivity as a parameter of signal detection, it is obvious to expect that this value increases as the particle size decreases. At this point, it is worth noting that "sensitivity" and "resolution" are not interchangeable terms. The former refers to the ability to detect one signal, while the latter is the ability to detect two signals as independent of each other. In all established SOPs, the maximum possible resolution point in the instrument was set.

As it was mentioned in materials and methods, the parameter "shutter" is the duration of the exposure to the video camera measured in the reciprocal of a second, and is inversely related with the number of the detected particles and the scattering intensity. The higher the shutter value, the smaller and darker the particles appear in the live view, which is useful to remove noise, particularly interesting for the measurement of larger particles by this method, as it is evidenced in our results.

Regarding the frame rate, it was stated before that this parameter indicates the number of recorded frames per time period (frames per second). Small particles move faster and require a higher frame rate in order to determine the diffusion coefficient of each individual particle and not to underestimate the mean square displacement. As expected, diffusion properties and thus the mean square displacement will be smaller for larger particles. Therefore, as the particle size increases, the resolution of the displacement can be improved by reducing the frame rate, which also agrees with our results.

Finally, post-acquisition parameters (minimum brightness, minimum area, maximum area, and trace length), present differences between the different SOPs. The values between the minimum and maximum area represent the gap of pixels that a particle contains to be analyzed in the statistics by the software. The maximum area was set as 1000 µm in all the SOPs. As we can see, as the size of the evaluated particles increases, the minimum area selected is greater. Thus, noise can be filtered out and only particles with an area of that size (measured in pixels) or larger are accepted. Objects with an area smaller than that are ignored in further analysis. This gains importance mainly during measurements of larger particles, where the suppression of small objects can increase the stability of the analysis and thus the precision of the result, matching the expected values. The same happens with the minimum brightness (adjusted minimum grey-value/ brightness of each particle). When the gray value is less than the threshold, the pixel will be black (background), which is also useful for reducing noise during the measurement of larger particles. Regarding the tracelength, which represents the number of frames that a particle is traced to be included in the analysis, the value decreases as the diameter of the evaluated particle increases as this parameter is also influenced by the movement of the particle to calculate the size more accurately, and smaller particles move faster. For obvious reasons, in none of the established SOPs the tracelength value (number of frames in which a particle is traced) was bigger than the number of total frames, which was set in every case as 90 (according to the highest resolution).

### 1.2 Calculation of the correction factor for each SOP established

A minimum of 10 measurements were made for SiO2 nanoparticles of 100, 200, 300, 400, and 500 nm using each of the established SOPs for the corresponding ideal range of particle size, as is shown in table 12. These measurements were made by setting "1" as the correction factor in the instrument, and the parameters established for each SOP (table 11) were not changed anymore.

Table 12: Measurements for the correction factor calculation.

SOP used	SiO2 nanoparticle used (nm)	Measurements	Size (nm)	Concentration measured (particles/ml)	Concentration expected (particles/ml)
SOP100_ExTu	100	13	101.3	5,57692 E+13	4,8E+13
SOP200_ExTu	200	12	199.98	4,94167 E+12	6E+12
SOP300_ExTu	300	10	242.27	1,72 E+12	1,8E+12
SOP400_ExTu	400	15	403.1	5,61333 E+11	7,5E+11
SOP500_ExTu	500	10	478.24	1,42 E+11	3,8E+11

Table 12. Measurements were made for calculating the concentration correction factor corresponding to each SOP established. The size and concentration measured are represented as the mean of the values obtained in all the measurements for each experiment. The expected concentration is the concentration given by the provider. The measurements are the number of experiments included in the analysis. The measurements are represented by the experiments included in the analysis and not the total experiments that were made.

SOP100\_ExTu was used for the measurement of 100 nm SiO2 nanoparticles (table 12). The mean of the concentration obtained from the 13 measurements considered was 5.58E+13 particles/ml with a standard deviation (SD) of +/- 4.7E+12 (data not shown) for an expected concentration (given by the provider) of 4.8E+13 particles/ml. The relation between the expected concentration and the concentration actually measured was used to calculate the concentration correction factor for SOP100\_ExTu, which was 0.81 (table 13. SD +/- 0.07, not shown).

For the measurement of 200 nm SiO2 nanoparticles using SOP200\_ExTu, the mean value for the concentration was 4.94E+12 particles/ml with an SD of +/- 9.4E+11 (not shown). Using the concentration given by the provider, the concentration correction factor calculated for SOP200\_ExTu was 1.26 (table 13) with an SD of +/- 0.25 (data not shown).

Ten measurements were made of 300 nm SiO2 nanoparticles using SOP300\_ExTu. The average concentration obtained for those measurements was 1.72E+12 particles/ml with an SD of 1.99E+11. The expected concentration (1.8E+12 particles/ml) allowed us to calculate a concentration correction factor of 1.06, (table 13) with an SD of +/- 0.12 (data not shown).

The SiO2 nanoparticles of 400nm were measured 16 individual times. One of the measurements had more than 3 positions removed by the software of the instrument and was considered an outlier, so only 15 measurements were included in our analysis. The reason for the positions removed was in all cases for "GRUBBS\_Number" (table 9), probably due to a heterogeneous distribution of the particles in the cell. The mean concentration for the 15 measurements included in the analysis was 5.61E+11 particles/ml with an SD of +/- 8.6E+10. The concentration correction factor was calculated again as the relation between the expected concentration (7.5E+11 particles/ml) and the mean concentration obtained, and the result was 1.37 with an SD of +/- 0,21.

Finally, SOP500\_ExTu was used for measuring 500 nm SiO2 nanoparticles. In this experiment, 12 measurements were made but 2 were excluded as outliers due to the same reasons as in the previous experiment (more than 3 positions removed by the software for GRUBBS\_Number). As we can see in table 12, the average concentration measured was 1.4E+11 particles/ml with an SD of +/- 1.03E+10 (not shown). Considering an expected concentration of 3.8E+11, the concentration correction factor calculated for SOP500\_ExTu was 2.69 (table13) with an SD of +/-0.19 (not shown).

Table 13: Concentration correction factors calculated for each SOP

Established SOP	SOP100_ExTu	SOP200_ExTu	SOP300_ExTu	SOP400_ExTu	SOP500_ExTu
Concentration correction factor	0.81	1.26	1.06	1.37	2.69

Table 13. The correction factor calculated for each SOP as the average of the relation between the concentration expected and the concentration actually measured was later included among the settings for the following measurements using the correspondent SOP.

Regarding particle diameter measurement, the mean values obtained in the different experiments were: 101.3 nm (SD +/- 1.86nm) using SOP100\_ExTu for the measurement of 100nm SiO2 nanoparticles, 199.98 nm (SD +/- 2.4nm) using SOP200\_ExTu for the measurement of 200nm SiO2 nanoparticles, 242.27nm (SD +/- 5.1nm) using SOP300\_ExTu for the measurement of 300nm SiO2 nanoparticles, 403.1 nm (SD +/- 8.56nm) using SOP400\_ExTu for the measurement of 400nm SiO2 nanoparticles, and 478.24 nm (SD +/- 11.81nm) using SOP500\_ExTu for the measurement of 500nm SiO2 nanoparticles. An example of the size distribution histograms for each experiment is shown in table 14.

Table 14. Example of size distribution histograms for each experiment during the calculation of the correction factors.

Experiment	Size distribution histogram	Statistical information
Measurement of 100 nm SiO2 nanoparticles using SOP100_ExTu.	1.2E+3" 1.1E+7" 1.0E+5" 9.0E+6 9.0E+6 9.0E+6 1.0E+6 1.0E+6 0.0E+8 0.0E+8 1.0E+6 0.0E+8	File name: 100_1_750000J  Peak analysis:  Diameter: 101,2 nm Particles/mL: 6.5E+6 X10: 72.2 X50 103.4 X90: 146.3 Span Mean: 0.7
Measurement of 200 nm SiO2 nanoparticles using SOP200_ExTu.	1.26+7 1.16+7 1.06+7 9.06+6 9.06+6 1.	File name: 200_1_111000_J  Peak analysis:  Diameter: 197,4 nm Particles/mL: 1,1E+7 X10: 140.2 X50: 190.1 X90: 254.3 Span Mean: 0.6
Measurement of 300 nm SiO2 nanoparticles using SOP300_ExTu.	1.86+7 1.66+7 1.46+7 1.24+7 1.14-7 1.	File name: 300_1_19980_J  Peak analysis:  Diameter: 241,3 Particles/mL: 1,5 E+7 X10: 165.2 X50: 230.1 X90: 295.3 Span Mean: 0,6
Measurement of 400 nm SiO2 nanoparticles using SOP400_ExTu.	1.06+0-7 9.05+6-8-8-8-8-8-8-8-8-8-8-8-8-8-8-8-8-8-8-8	File name: 400_1_15000J  Peak analysis:  Diameter: 399,2 nm Particles/mL: 6,9E+6 X10: 281.6 X50: 377.5 X90: 469.6 Span Mean: 0.7
Measurement of 500 nm SiO2 nanoparticles using SOP500_ExTu.	1.06+7-7-80+6-6-8-8-8-8-8-8-8-8-8-8-8-8-8-8-8-8-8-8	File name: 500_1_3000K  Peak analysis:  Diameter: 465,8 nm Particles/mL: 6,8E+6 X10: 275.2 X50: 442.3 X90: 569.6 Span Mean: 0,8

Table 14. Schematic exemplification of the distribution histograms obtained in each experiment included in the calculation of the correction factors. The file name in each case is represented by the size of the measured particle and the final dilution used. Statistical information of the peak analysis: X10 = 10% of all analyzed particles are smaller than the stated value; X50 = 50% of all analyzed particles are smaller and 50% are larger than the stated value; X90 = 90% of all analyzed particles are smaller than the stated value; Span: Measure of the width of the distribution and it is calculated from (X90-X10) / X50

Due to a large amount of data, histograms obtained during all measurements are not shown. However, all measurements made with the same SOP for particle size within the ideal size range show similar distribution characteristics. The Span mean, of all measurements of 100

nm SiO nanoparticles made using SOP100\_ExTu, 200nm diameter using SOP200\_ExTu, and 300nm diameter using SOP300\_ExTu, was 0.6. In the case of the 400 nm beads measurements, performed with SOP400\_ExTu, it was 0.7, while for 500nm + SOP500\_ExTu it was 0.8. The fact that this parameter, which represents how wide the size dispersion is, has almost the same value during ten measurements, would indicate not only precision to measure the size of the particle, but also linearity of the results.

In addition, these results evidenced that the larger the particle diameter, the larger the particle size measured, the wider the base of the histogram, probably indicating greater variability in the particle size measured in each experiment (which coincides with the increasing standard deviation values).

## 1.3 SOPs cross-compatibility evaluation.

It was previously stated that these SOPs were established for a particular size of particle, meaning by that that there is an ideal size range of particle for each SOP. At this step, the performance of each SOP for measuring particles beyond the ideal size range was evaluated and is what it was defined as crossed compatibility. To achieve this, the established SOPs were used for the measurement of SiO2 nanoparticles of different diameters, in a minimum of 10 measurements for each size (table 15).

Measurements of 100nm SiO2 nanoparticles using SOP400\_ExTu were possible but not in a reliable way. A final dilution of 1: 50000 was made obtaining an accurate number of detected particles and calculated concentration, but all the positions were removed by the software by "Min\_Traces" (too few particles in the field of view) and analysis could not be done. The same result was for dilutions 1:25000 and 1:20000. Using a dilution factor of 1:10,000, measurements could be carried out. However, in most cases, more than three positions were removed or the number of particles detected was too high, compromising image resolution. Measurement of 100 nm silica beads using SOP500\_ExTu, was not possible. The first dilution of 1:500 with a final volume of 1 ml was made and from there, a second dilution was made to obtain the final dilution. Seven final dilutions were tried but none of the measurements had reliable results. In each case, all the positions were removed by the software for Min\_Traces. In tables 16 and 17, the measurement of 100, 200, 300, 400, and 500 nm using SOP100\_ExTu is illustrated with an example of each experiment.

Table 15.SOPs cross-compatibility

SOP used	SiO2 nanoparticle	Measurements	Size measured	Concentration measured	Expected concentration
	used (nm)		(nm)	(particles/ml)	(particles/ml)
	100	13	97.82	4,4E+13	4,8E+13
	200	11	186.58	1,66364E+13	6E+12
SOP100_ExTu	300	10	Not possible	3,65E+12	1,8E+12
	400	12	Not possible	3,91667E+12	7,5E+11
	500	11	Not possible	4,37273E+11	3,8E+11
	100	10	119.12	2,64E+13	4,8E+13
	200	11	201.01	1,08E+13	6E+12
SOP200_ExTu	300	11	247.23	2,86364E+12	1,8E+12
	400	15	377.05	2,58E+12	7,5E+11
	500	12	419.54	3,41667E+11	3,8E+11
	100	14	133.92	4,44286E+12	4,8E+13
	200	12	197.05	7,25E+12	6E+12
SOP300_ExTu	300	12	247.09	1,76667E+12	1,8E+12
	400	10	379.76	2,23E+12	7,5E+11
	500	14	423.1	2,9E+12	3,8E+11
	100	16	100.35	1,6E+12	4,8E+13
	200	12	201.45	2,95385E+12	6E+12
SOP400_ExTu	300	15	255.88	9,86E+11	1,8E+12
	400	15	363.07	8,7E+11	7,5E+11
	500	11	447.73	1,36364E+11	3,8E+11
	100	13	Not possible	Not possible	4,8E+13
	200	26	186.38	8,46923E+12	6E+12
SOP500_ExTu	300	13	254.48	2,12308E+12	1,8E+12
	400	12	397.57	3,38333E+12	7,5E+11
	500	10	465.32	4,5375E+11	3,8E+11

Table 15. Data obtained from using the different SOPs the measurement of each SiO2 nanoparticle. The number of measurements is represented by those included in the final analysis and not the total that were made. The difference between the expected concentration and the concentration measured, can be observed in each case.

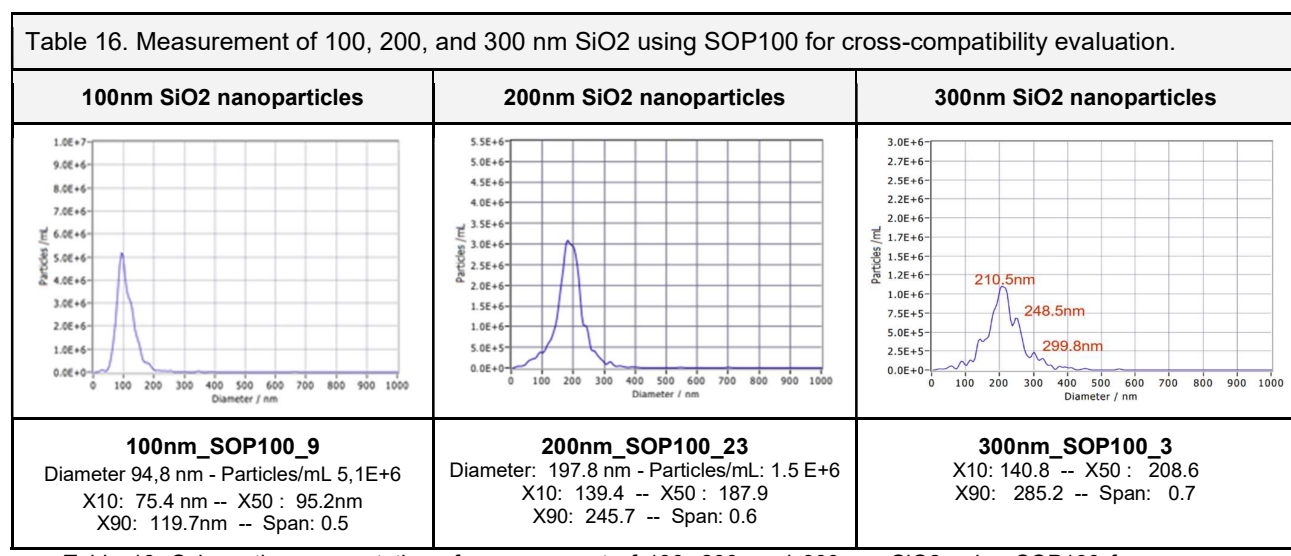


Table 16. Schematic representation of measurement of 100, 200, and 300 nm SiO2 using SOP100 for cross compatibility evaluation. The table shows the SOP and particle size used in the exemplified measurement, the name of the file (represented by the particle size, the the SOP and the number of measurement), the size distribution histogram and the statistical data of the peak analysis.

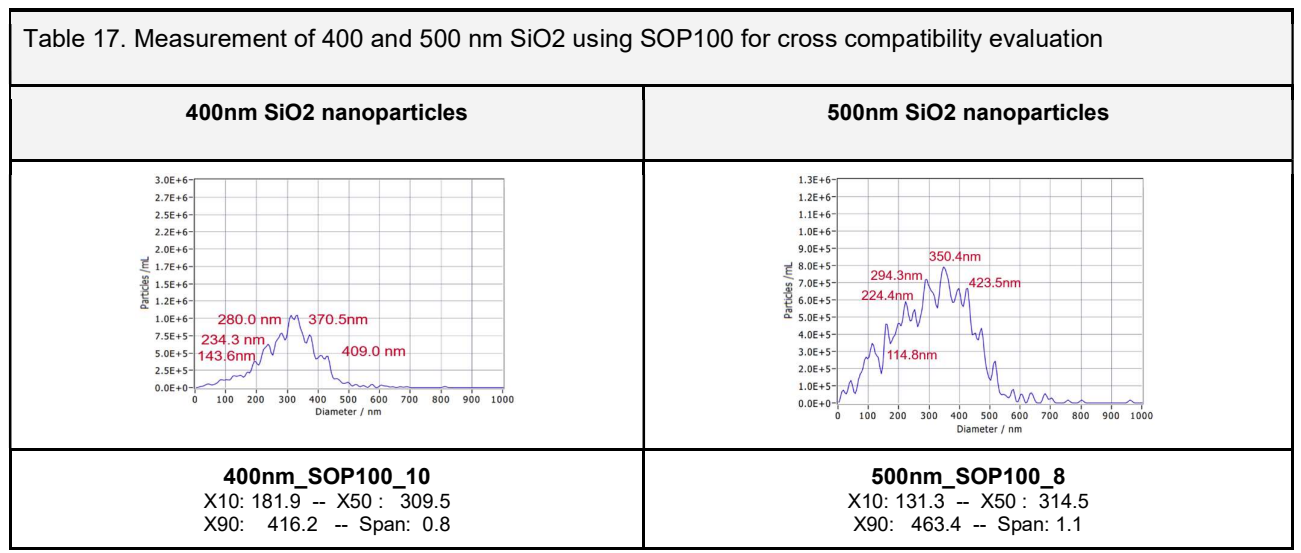


Table 17. Schematic representation of measurement of 400 and 500 nm SiO2 using SOP100 for cross compatibility evaluation. The table shows the SOP and particle size used in the exemplified measurement, the name of the file (represented by the particle size, the the SOP and the number of measurement), the size distribution histogram and the statistical data of the peak analysis.

As it is shown in table 15 and in the size distribution histograms, the diameter measurement was not possible for SiO2 nanoparticles of 300, 400 and 500 nm when using SOP100\_ExTu due to the multiples peaks in the histogram (a situation that is worst as the larger the particle size). This can be explained through the difference in the parameters set in the different SOPs. With the concept that NTA is an optical method that uses the light scattered by each of the particles in suspension in motion, it is obvious that the measurement of smaller particles requires more "attention" or work on the part of the instrument. As the light scattered by the smaller particles is smaller, a higher sensitivity and a lower brightness threshold is required. In addition, these particles move faster, so they require a longer exposure time to the camera to be analyzed correctly and, as previously mentioned, to achieve this we decrease the shutter value and increase the frame rate and the tracelength. This is what happens with the SOP100 ExTu, which was set for the measurement of 100-nanometer particles. When we use this SOP for the measurement of larger particles, the instrument cannot measure them properly because the background noise consumes too much work and most of the attention is diverted to the measurement of smaller particles that may be present. On the other hand, the SOP500 ExTu was established for the measurement of particles ideally 500nm in diameter and in its settings, the background noise is muted (lower sensitivity, higher brightness threshold, higher shutter, lower tracelength, etc). This helps to understand why as the particle size increases, the measurement with the SOP100 ExTu becomes less accurate. The same thing happens, but in reverse, when measuring small particles using the SOP500 ExTu, which has a detection threshold too high to sense them.

Table 18. Measurement of 100, 200, and 300 nm SiO2 nanoparticles using SOP200 for cross-compatibility evaluation.

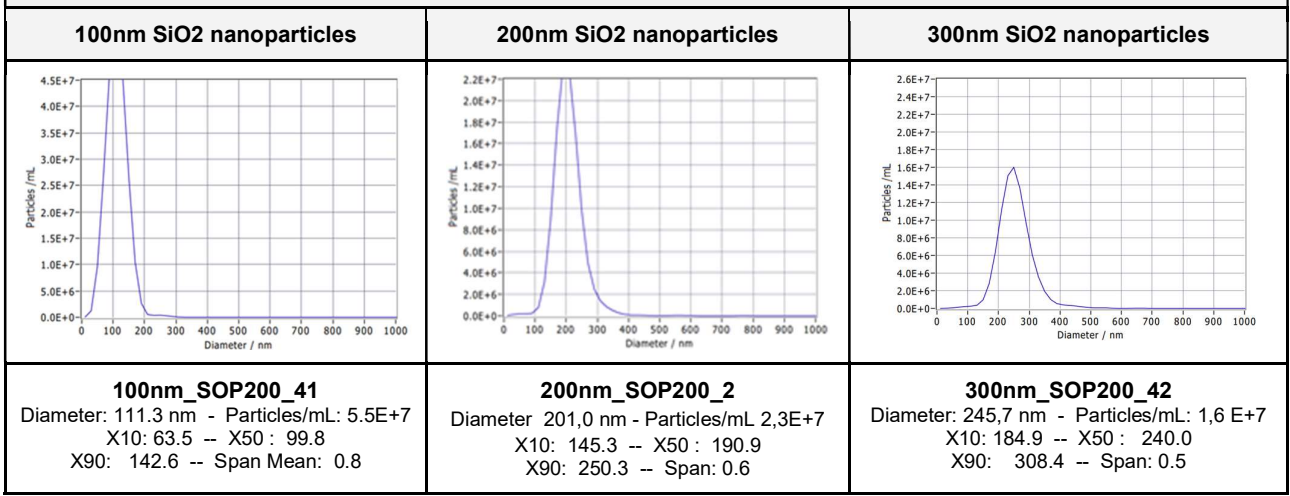


Table 18. Schematic representation of measurement of 100, 200, and 300 nm SiO2 using SOP500 for cross compatibility evaluation. The table shows the SOP and particle size used in the exemplified measurement, the name of the file (represented by the particle size, the the SOP and the number of measurement), the size distribution histogram and the statistical data of the peak analysis.

SOPs 200, 300 and 400\_ExTu (tables 18 to 23 and table 26), seem to overlap in the range of sizes that can be measured. By using any of these SOPs, 100nm particles can be measured. However, the concentration is increasingly underestimated (represented by the high error precision factors in table 26), and since both parameters, size and concentration influence each other's measurement result, we can afirm that the measurement of 100 nm particles using SOP400\_ExTu is neither accurate nor appropriate, for the same explained reasons that for using SOP500 ExTu.

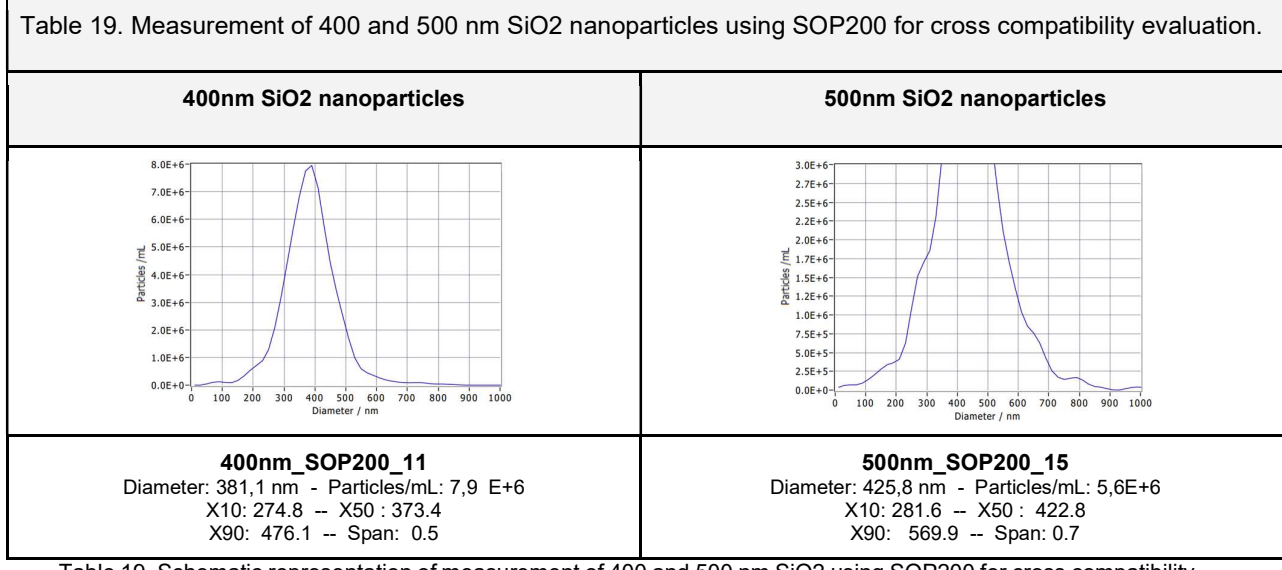


Table 19. Schematic representation of measurement of 400 and 500 nm SiO2 using SOP200 for cross compatibility evaluation. The table shows the SOP and particle size used in the exemplified measurement, the name of the file (represented by the particle size, the the SOP and the number of measurement), the size distribution histogram and the statistical data of the peak analysis.

Table 20. Measurement of 100, 200, and 300 nm SiO2 nanoparticles using SOP300 for cross compatibility evaluation.

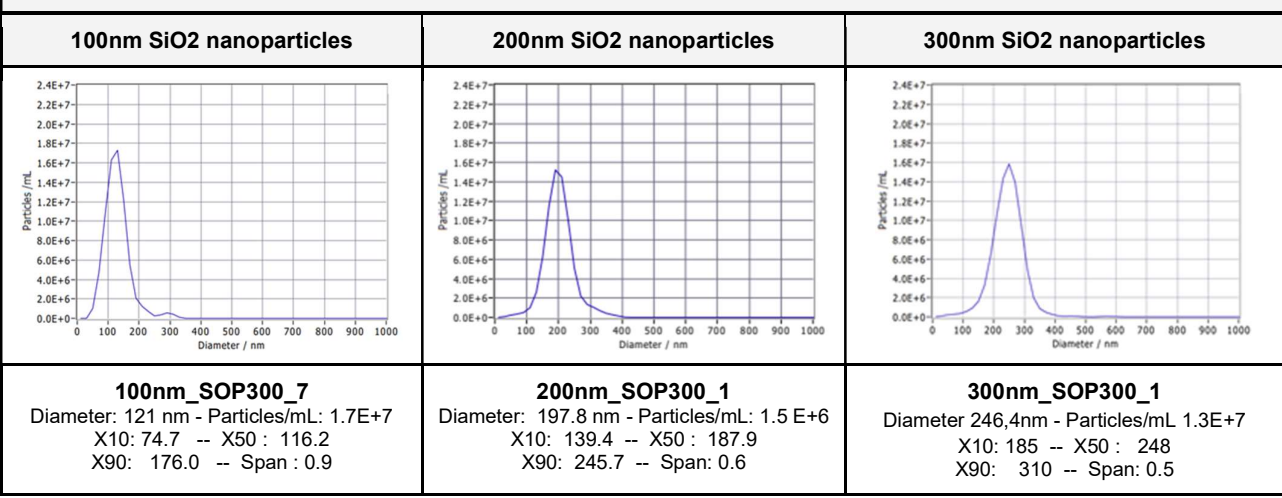


Table 20. Schematic representation of measurement of 100, 200, and 300 nm SiO2 using SOP300 for cross compatibility evaluation. The table shows the SOP and particle size used in the exemplified measurement, the name of the file (represented by the particle size, the the SOP and the number of measurement), the size distribution histogram and the statistical data of the peak analysis

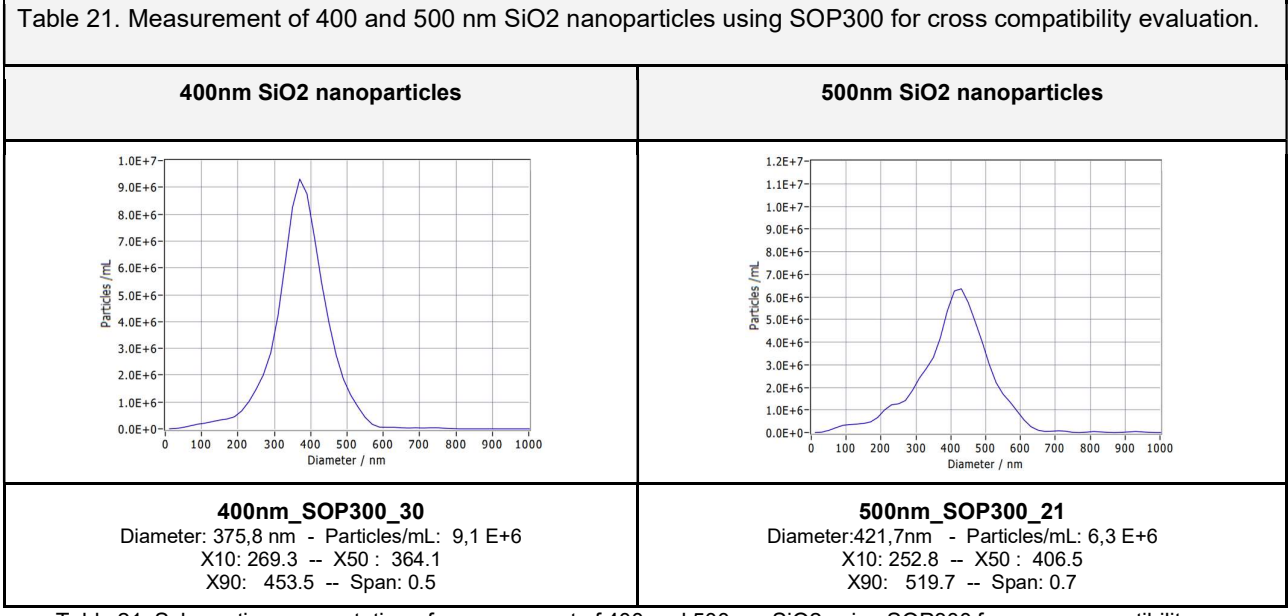


Table 21. Schematic representation of measurement of 400 and 500 nm SiO2 using SOP300 for cross compatibility evaluation. The table shows the SOP and particle size used in the exemplified measurement, the name of the file (represented by the particle size, the the SOP and the number of measurement), the size distribution histogram and the statistical data of the peak analysis.

Our results demonstrate that the size distribution measurement for 300nm SiO2 nanoparticles (also 400 and 500) is underestimated even when the SOP used is the established for that size (SOP300\_ExTu). We can assume at this point, that the reason for that is because the particle is actually smaller than 300nm or due to a bigger polydispersity than the given by the provider.

Table 22. Measurement of 100, 200, and 300 nm SiO2 nanoparticles using SOP400 for cross compatibility evaluation.

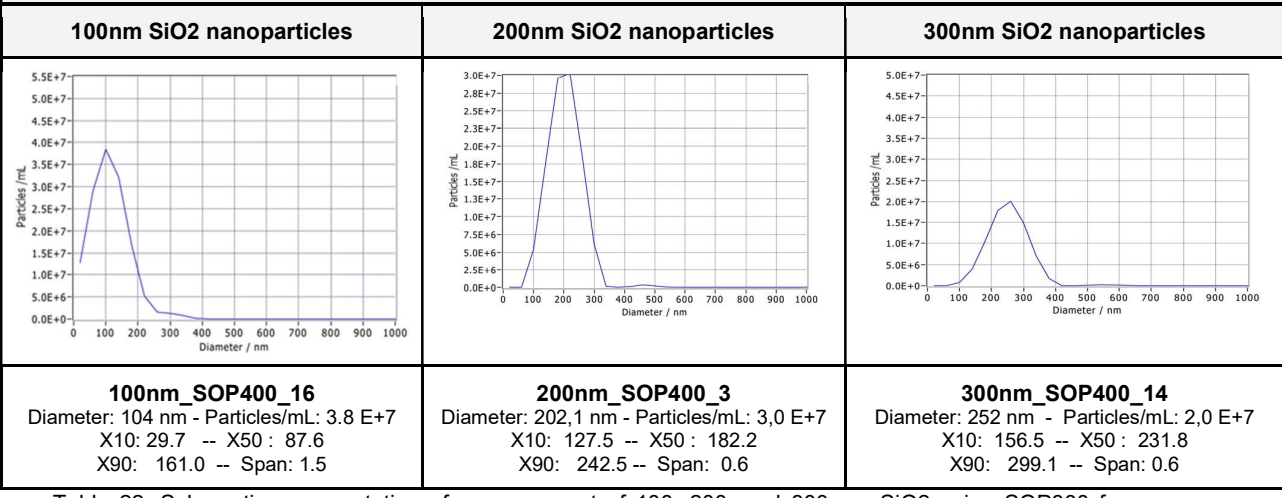


Table 22. Schematic representation of measurement of 100, 200, and 300 nm SiO2 using SOP300 for cross compatibility evaluation. The table shows the SOP and particle size used in the exemplified measurement, the name of the file (represented by the particle size, the the SOP and the number of measurement), the size distribution histogram and the statistical data of the peak analysis

Table 23. Measurement of 400 and 500 nm SiO2 nanoparticles using SOP400 for cross compatibility evaluation.

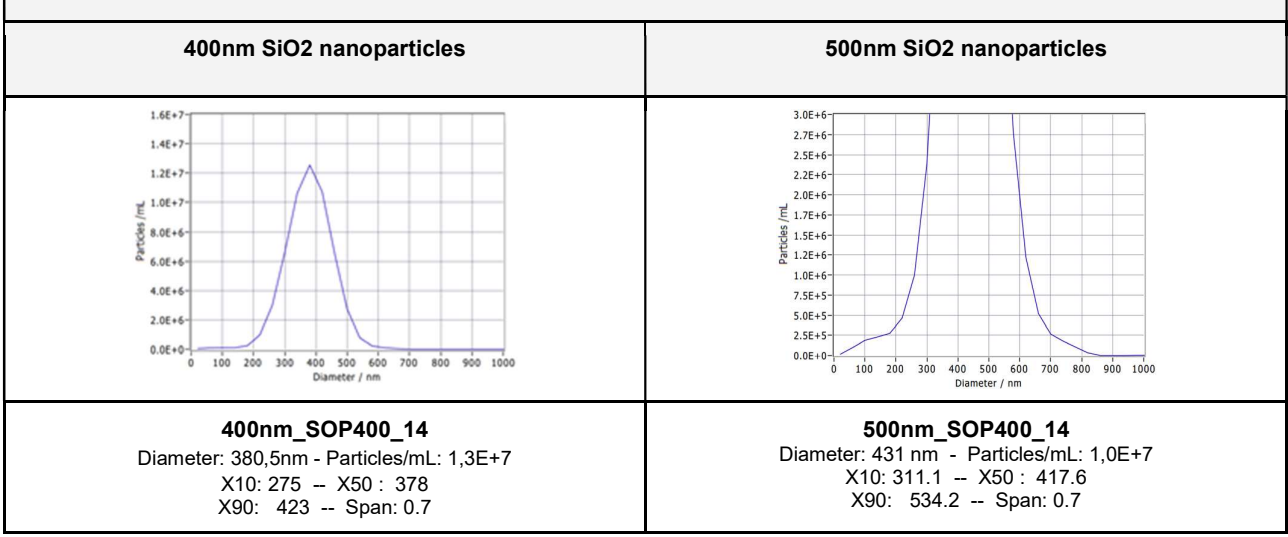


Table 23. Schematic representation of measurement of 400 and 500 nm SiO2 using SOP400 for cross compatibility evaluation. The table shows the SOP and particle size used in the exemplified measurement, the name of the file (represented by the particle size, the the SOP and the number of measurement), the size distribution histogram and the statistical data of the peak analysis.

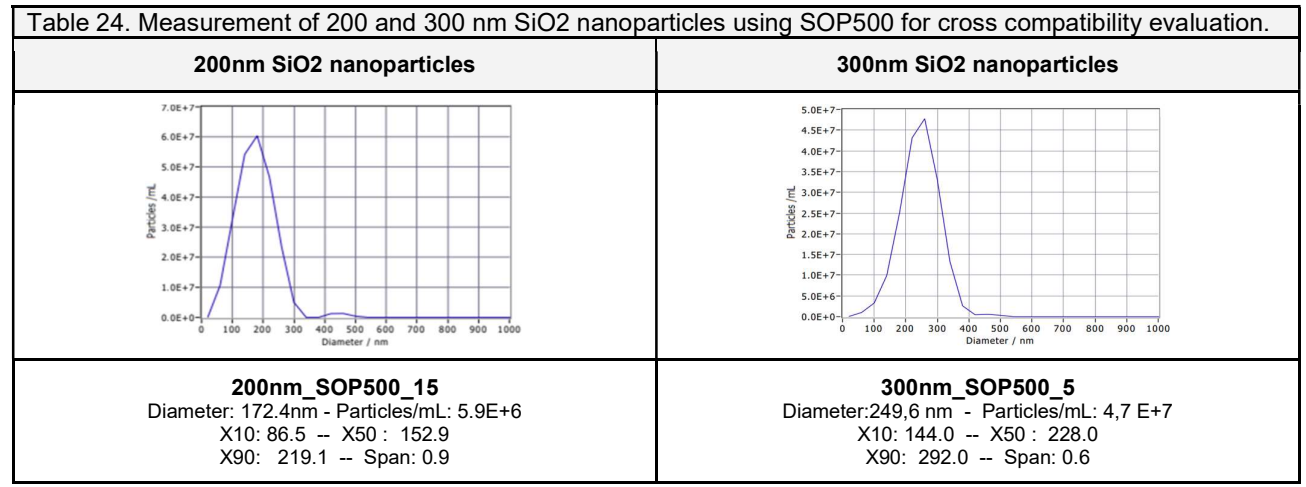


Table 24. Schematic representation of measurement of 100, 200, and 300 nm SiO2 using SOP500 for cross compatibility evaluation. The table shows the SOP and particle size used in the exemplified measurement, the name of the file (represented by the particle size, the the SOP and the number of measurement), the size distribution histogram and the statistical data of the peak analysis

The results obtained by the measurement of particles of 400 and 500 nm, regardless the SOP used in the experiment, evidenced wider base of the size distribution histograms (supported by the statistical data, as it was previously mentioned), meaning by this also that there is more polydispersity in the sample, or that is more difficult for the instrument the measurement of larger particles.

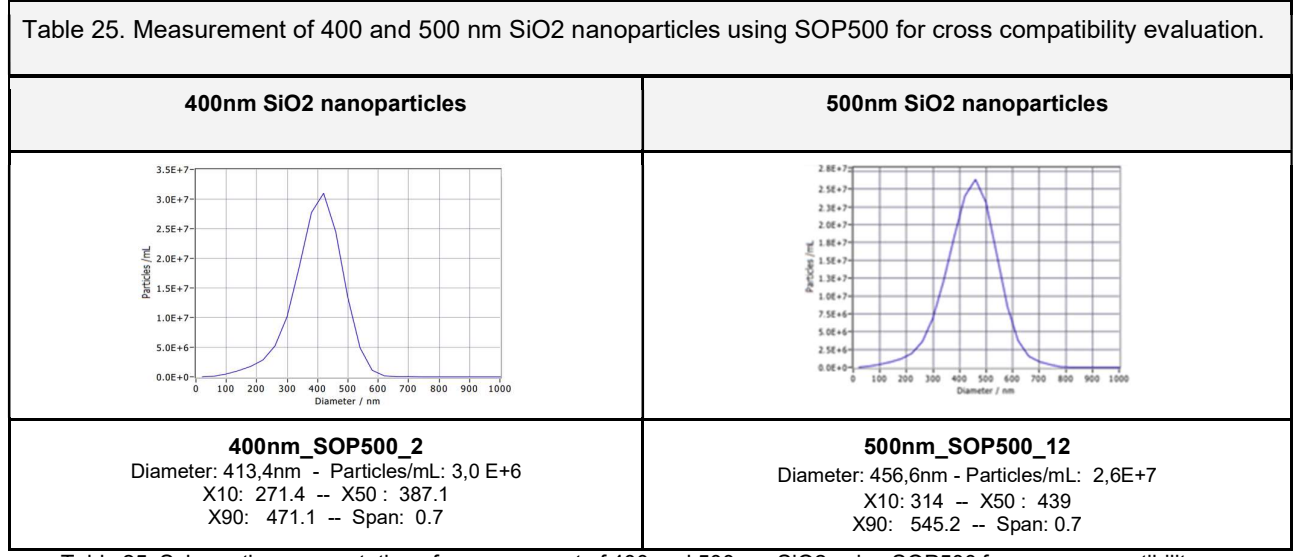


Table 25. Schematic representation of measurement of 400 and 500 nm SiO2 using SOP500 for cross compatibility evaluation. The table shows the SOP and particle size used in the exemplified measurement, the name of the file (represented by the particle size, the the SOP and the number of measurement), the size distribution histogram and the statistical data of the peak analysis.

In every experiment made at this point, the relation between the expected concentration and the concentration actually measured, was used to calculate the "error precision factor" as a parameter of compatibility between the established SOPs and SiO2 nanoparticles of different sizes. Since these SOPs had the concentration correction factor, we expected that the stok concentration and measured concentration were closer at this point, represented by an error precision factor closer to 1 than the correction factor, especially when measuring again particles within the ideal size range. Table 26 summarizes the error precision factors calculated for each experiment

Table 26. Error precision factor obtained in the SOP cross-compatibility evaluation

Error precision factor										
	Silica Beads per size									
		100nm 200nm 300nm 400nm 500n								
	SOP100_ExTu	1,11	0,36	0,52	0,19	0,87				
	SOP200_ExTu	1,86	0,56	0,64	0,29	1,1				
SOP	SOP300_ExTu	11,18	0,82	1,02	0,34	1,25				
	SOP400_ExTu	31,52	2,03	1,84	0,88	2,82				
	SOP500_ExTu	Not possible	0,72	0,87	0,22	0,84				

As it can be observed, the measurement of 200 nm SiO2 nanoparticles using SOP200\_ExTu (correction factor is 1.26) and the measurement of 400nm SiO2 nanoparticles using SOP400\_ExTu (correction factor 1.37) had, as a result, the worst relationship between the stock concentration and the concentration measured, reflected by the value of error precision factor, which is farther to "1" than the correction factor in both cases, and these SOPs need an improvement.

# 1.4 Measurement of SiO2 nanoparticles of 30, 50, 70, and 150 nm using the established SOPs.

To determine with more precision the size range of detection of the established SOPs, additional measurements were made using SiO2 nanoparticles smaller than 100nm (30, 50, and 70nm). Since the experiments made using SOP500\_ExTu have shown that this SOP is sensitive enough to detect particles of 200 nm diameter but not 100 nm particles, at this step, SiO2 nanoparticles of 150 nm were also included in the experiment.

Firstly, the measurement of particles of 150 nm diameter was carried out by using SOP100\_ExTu and the concentration was overestimated, as we expected. The average concentration obtained was 3E+14 (SD: +/-1.5E+12) for a stock concentration of 1.4E+14 (given by the provider). The best results were obtained using the SOP200\_ExTu for the measurement of this particle size, considering both size and concentration.

Table 27. Measurement of smaller SiO2 nanoparticles using the established SOPs.

					SiO2 na	anoparticle	e used per size					
	1	50nm		70nm		50nm			30nm			
SOP used	Concentration in particles/ml (Mean)	Diameter (mean)	Error precisio n factor	Concentration in particles/ml (Mean)	Diameter (mean)	Error precisio n factor	Concentration in particles/ml (Mean)	Diamete r (mean)	Error precisio n factor	Concentration in particles/ml (Mean)	Diamete r (mean)	Error precisio n factor
SOP100 ExTu	3E+14 SD +/- 1,5E+12	133,5 nm SD+/-4.5	0,46	2.1E+13 SD+/- 4,1E+12	74,6 nm SD+/- 3,4	3,42	2.4E +12 SD +/- 2E+12 nm SD+/-					
SOP200 ExTu	1,6E+13 SD +/- 1E+12	143,8 nm SD+/-6,2	0,86	9.8E +11 SD +/- 7E+11	123nm SD +/-3	117						
SOP300 ExTu	9E+12 SD +/- 1,5E+12	145 nm SD+/-7,6	1,6			Not made			Not made.			
SOP400 ExTu	1,1E+13 SD+/- 2E+12	Not posible	1.38	Not made.					Not made			
SOP500 ExTu	Not	possible.										

Table 27. Statistical data were obtained from the measurements of each SOP-particle combination. Measurement of 150nm particles using SOP500\_ExTu was attempted but not possible for Min\_Traces. The measurement of 70nm particles from SOP300\_ExTu, 50nm particles from SOP200\_ExTu, and 30nm from SOP100\_ExTu inclusive, was not made.

The concentration measured when using SOP400\_ExTu was 1.1E+13 resulting in an error precision factor of 1.38, but the size distribution could not calculate the diameter due to multiples values, as it is illustrated in the histograms.

The measurement of this particle using SOP500\_ExTu was tried with different final dilutions but in any case, was possible. Every time all the positions were removed by Min\_Traces.

Then, 70nm SiO2 particles were measured. The average diameter measured and the correspondent size distribution histogram obtained by using SOP100\_ExTu was precise, but the concentration was underestimated, reflected in an error precision factor of 3.42 (concentration measured: 2.1E+13, for a stock concentration of 7E+13).

The measurement of this particle size using SOP200\_ExTu was attempted with several final dilutions but neither the size nor the concentration was accurate and in most of the measurements included in the experiment all the positions were removed due to Min\_Traces. An example of a size distribution histogram obtained from the measurement of 70nm SiO2 nanoparticles using SOP100\_ExTu and SOP200\_ExTu, is illustrated in table 29.

Table 28. Size distribution histograms in the measurement of 150nm SiO2 nanoparticles using different SOPs.

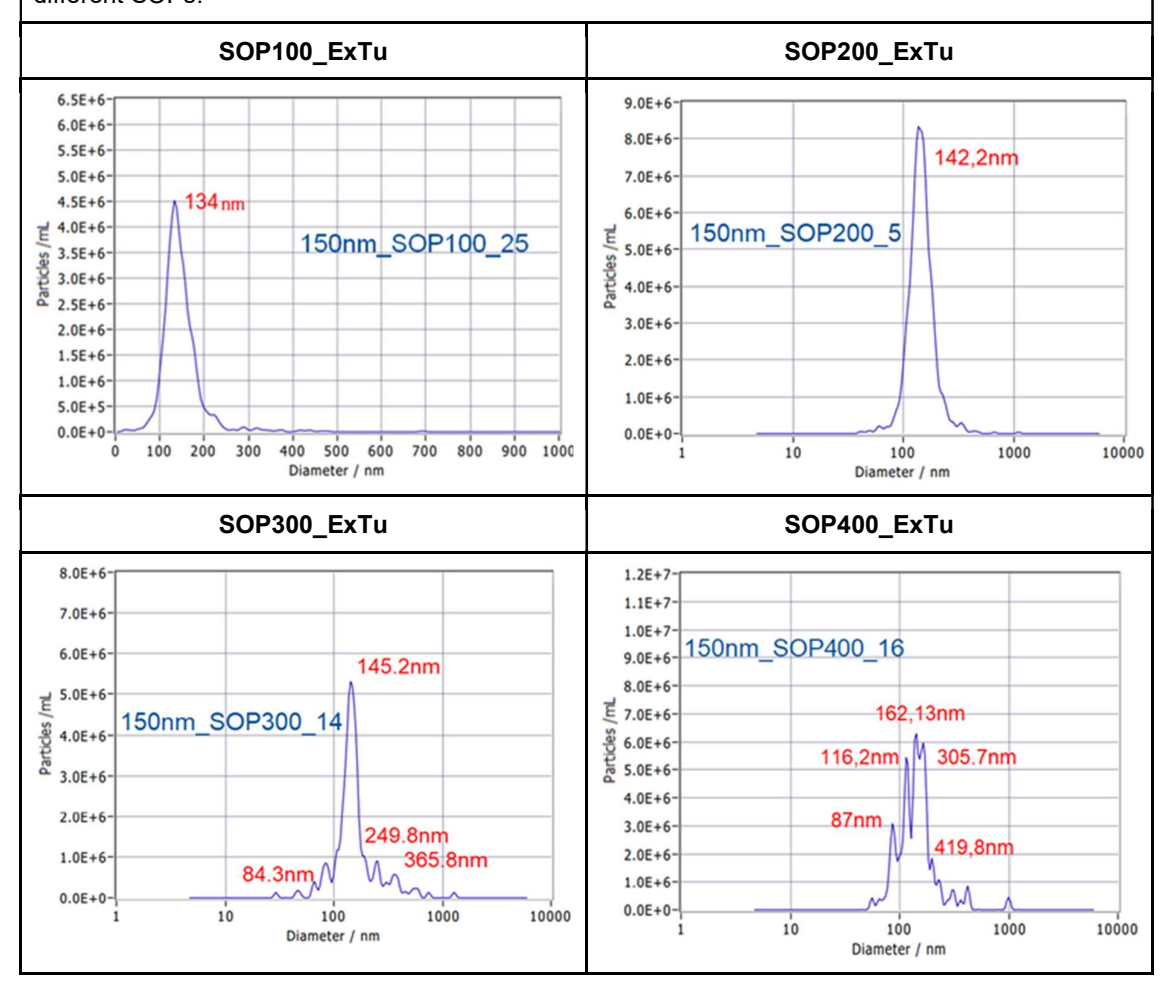
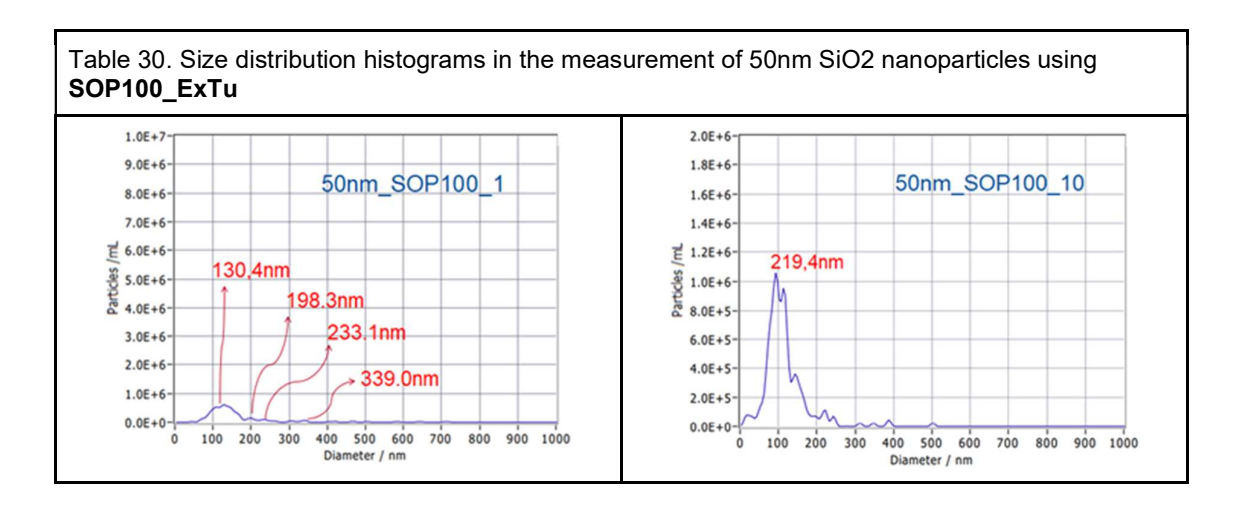


Table 29. Size distribution histograms in the measurement of 70nm SiO2 nanoparticles using different SOPs. SOP100\_ExTu SOP200\_ExTu 7.0E+6 1.0E+7 73,7nm 9.0E+6 70nm\_SOP200\_1 6.0E+6 8.0E+6 5.0E+6 7.0E+6-70nm\_SOP100\_12 ₹ 4.0E+6 6.0E+6 5.0E+6 3.0E+6 4.0E+6 2.0E+6 3.0E+6 2.0E+6 1.0E+6 1.0E+6-341.9nm 515.3nm 833.6nm 0.0E+0-0.0E+0-10 100 1000 10000 400 500 600 700 800 900 1000 Diameter / nm Diameter / nm

Finally, the measurement of 50nm SiO2 nanoparticles using SOP100\_ExTu was attempted. Several final dilutions were tried but most of the time all the positions were removed due to min\_traces, and the measurements that could be made had bad results in both size and concentration. Table 30 illustrates two examples of size distribution histograms obtained from the measurement of 50nm SiO2 nanoparticles using SOP100\_ExTu



The measurement of 30 nm SiO2 particles was considered not worthwhile and was not performed with any of the SOPs. Our results in this experiment allow us to conclude two things: On the one hand, the detection threshold of the SOP500\_ExTu is around 200 nm, since 100 and 150-nanometer particles could not be measured with this SOP. On the other hand, it is demonstrated that particles smaller than 100 nm are outside the detection range of the established SOPs and a new SOP for these particles will be necessary to create in future experiments.

# 1.5 EVs measurement using the established SOPs

EVs were isolated by SEC and TFF from cell culture. Previously, cells were counted, the percentage of viability was calculated, and mycoplasma contamination was discarded. A total of 3 steps of centrifugation were made: for cell aggregates detachment, for removal of cell debris, and for size separation. After the last centrifugation, the pellet was resuspended in PBS (5ml), and used to carry out TFF for the isolation of EVs large (larger than 200nm). As an intermediate step for EVs large isolation, a concentration of the sample using 100kDa X-Spinner tubes was used. The supernatant from the cell culture last centrifugation was concentrated using a 100kDa chamber membrane and then used for the small EVs isolation by SEC. A total of 8 fractions (F1 - 8) were isolated and the void volume (VV).

A total of 13 samples were isolated: 8 SEC fractions, void volume, EV large (TFF retentate), and the flowthrough TTF, 100kDa chamber membrane and 100kDs X-Spinner tube. All the samples obtained were aliquoted for characterization using NTA and microBCA.

Tables 17, 18, and 19 summarize the concentration obtained from the NTA measurements of the different aliquots.

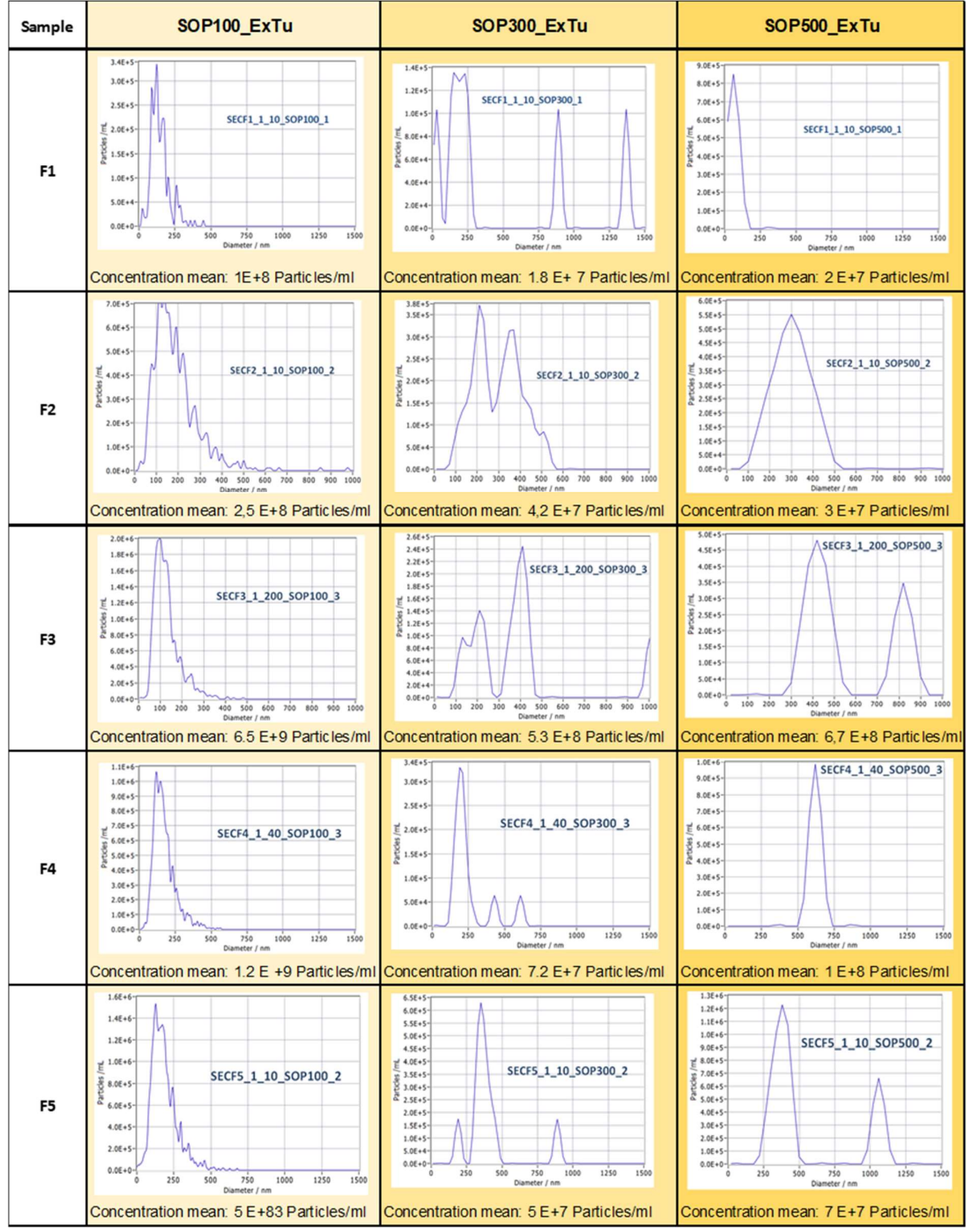


Table 31. NTA measurements of SEC fractions 1 - 5

Table 31. Measurement of SEC fractions 1-5 using SOP100\_ExTu, SOP300\_ExTu, and SOP500\_ExTu. The concentration shown here, is represented by the mean of the results obtained for each measurement, and expressed in particles/ml.

Table 32. NTA measurements: SEC fractions 6 - 8, VV and flowthrough 100 kDa chamber membrane

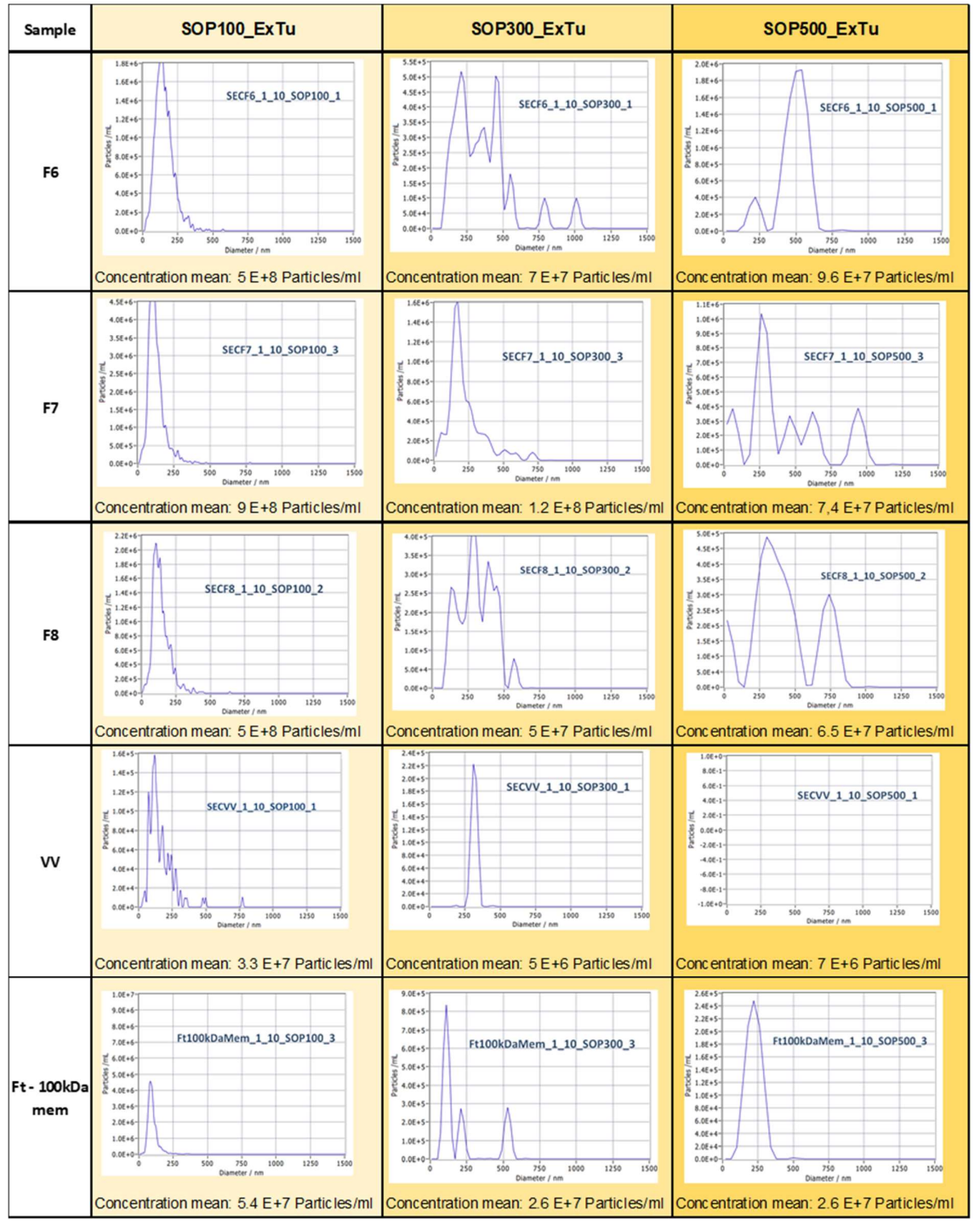


Table 32. Measurement of SEC fractions 6 - 8, VV and flowthrough 100 kDa chamber membrane using SOP100\_ExTu, SOP300\_ExTu, and SOP500\_ExTu. The concentration obtained for each measurement is in particles/ml.

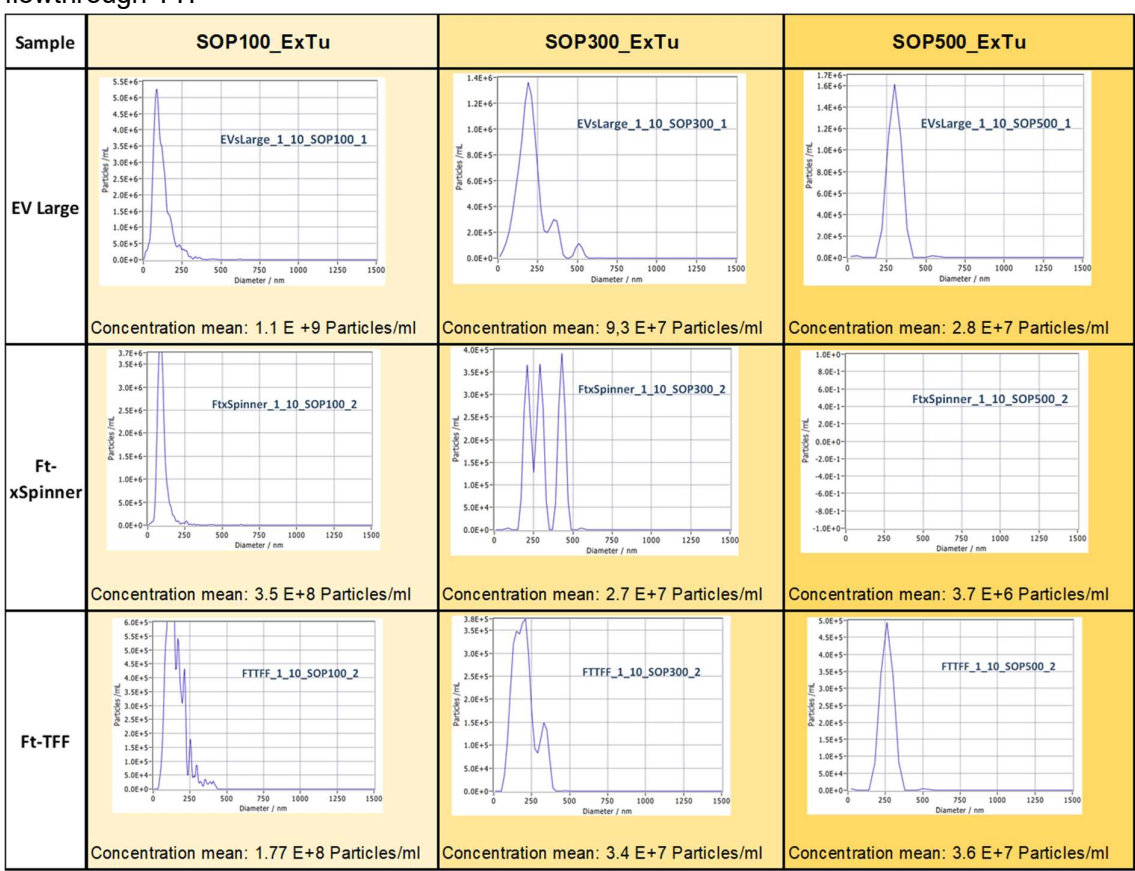


Table 33. NTA measurements of EV large, flowthrough 100 kDa X-Spinner tube and flowthrough TTF

Table 33. Measurement of EV large, flowthrough 100 kDa X-Spinner tube and flowthrough TTF, using SOP100\_ExTu, SOP300\_ExTu, and SOP500\_ExTu. The concentration obtained for each measurement is in particles/ml.

Our results show that the highest concentration of EVs is found in fractions 3 and 4 of the SEC isolation (mean of concentration values: 6.5E+9 and 1.2E+9 particles/ml respectively), followed by the aliquot of large EVs isolated by TFF.

All measurements performed with SOP500\_ExTu resulted in the removal of all positions because very few particles were detected in the field of view (Min\_Traces). They were manually attached for analysis. However, the concentration obtained using this SOP was not sufficient, even when measuring EV large, which might also suggest that isolation methods at this particle size should be improved.

In addition, the measurement of all samples analyzed showed great intra- and inter-experiment variability (as can be seen in the size distribution histograms) when using the SOP300\_ExTu and SOP500\_ExTu. On the other hand, when using SOP100\_ExTu, linearity can be observed in the results, both inter and intra-experiments.

When comparing the relationship between the concentration obtained by NTA and the protein content of each sample by microBCA, it was evident that the highest protein content is found in the flow through the 100kDa membrane of the concentration chamber.

### 1.6 Determination of total protein contained in the isolated samples

After performing the quantification of the particles contained in each cell culture isolation sample, the total protein contained in them was evaluated. As previously mentioned, the NTA in scatter mode measures the concentration and size of suspended particles, without differentiating between other co-isolated particles (protein and lipoprotein aggregates) and the particles of interest (EVs). In this sense, when determining the protein content, it is possible to differentiate between a well-performed particle isolation and an inadequate one.

To achieve the goal of ruling out protein contaminants, we performed a MicroBCA assessment (Thermo Scientific, USA) to quantify the total free protein concentration. This assay detects the free protein and the protein of the vesicles themselves, evidencing successful and adequate isolation of the vesicles by decreasing the levels of protein contained per fraction.

The highest protein content in our samples was obtained by the 100kDa membrane flowthrough from the concentration chamber, followed by fraction 8 from the SEC isolation and the TFF flowthrough. Our results suggest adequate purification of vesicles and separation of contaminants from non-EV material in all tested isolate samples tested. This result was observed by a difference in the protein concentration in the fractions, when they contain a higher yield of particles, they show a decreased protein concentration, and vice versa, when low particles are expressed, more protein is detected.

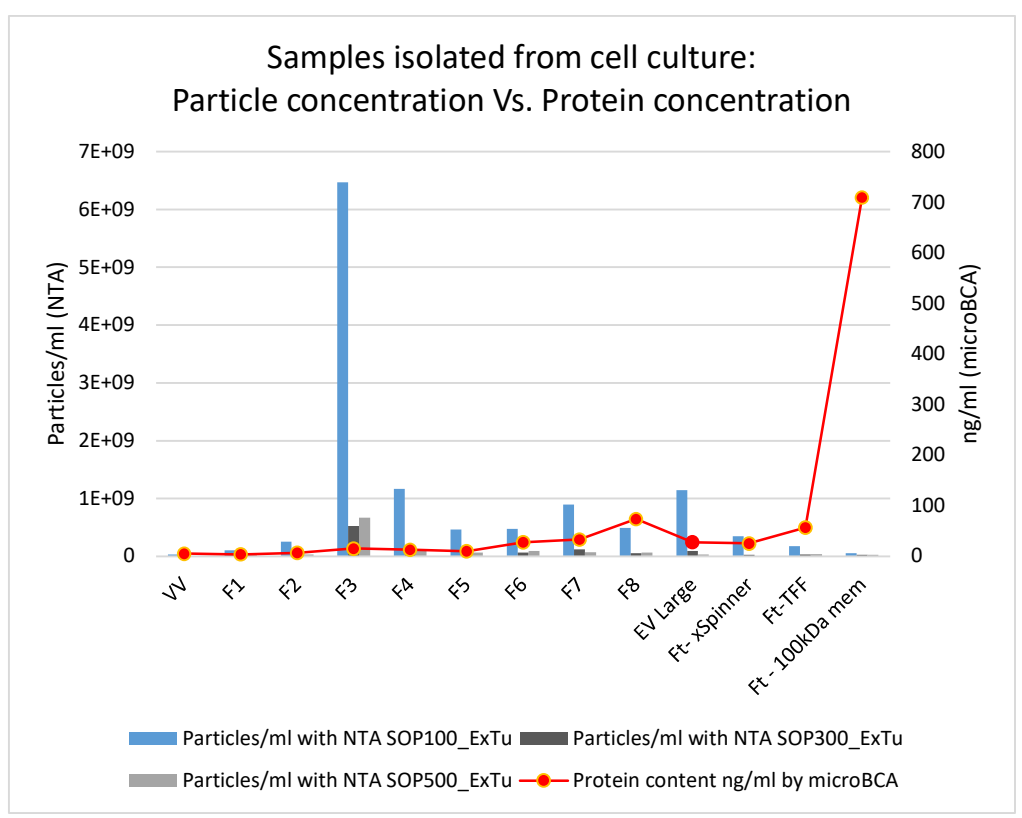


Figure 10. Determination of particle concentration (SOP100\_ExTu, SOP300\_ExTu, and SOP500\_ExTu) Vs quantification of total protein (ng/mL) of all isolated samples. are shown. The number of particles and the protein concentration do not increase simultaneously, confirming the successful isolation and purification of particles.

# 2. Measurement of reference material and EVs using NTA in fluorescent mode

### 2.1 Establishment of the SOP in fluorescent mode.

In order to create a new SOP for fluorescent mode, parameters were decided using the NTA manufacturer recommendations. By measuring NTA fluorescent standard (polystyrene fluorescent beads of 100nm diameter) The final dilution for the measurements was decided considering that the number of detected particles were in the ideal range (50 - 200).

New SOP name	SOP488_ExTu_fluo			
	Sensitivity	80		
	Schutter	100		
	Frame Rate	30		
	Positions	11		
	Cycles	1		
	Resolution	Highest		
	Min Brightness	30		
	Min Area	10		
Parameters	Max Area	1000		
at the same and th	Trace Length	10		
	Tracking radius	100		
	nm/class	5		
	Size/class	64		
	Temperature	25		
	Select Laser	488		
	Fluorescent filter	500nm		

Table 34. Settings of SOP established for measurements using NTA in fluorescent mode.

### 2.2 Relative correction factor calculation

100nm green fluorescent PS nanoparticles were diluted in ddH2O in a 1:1000000 final dilution. Each sample was measured two times: first, using the new SOP for fluorescent mode (SOP488\_ExTu\_fluo) and then using SOP100\_ExTu (SOP for 100nm diameter particles in scatter mode).

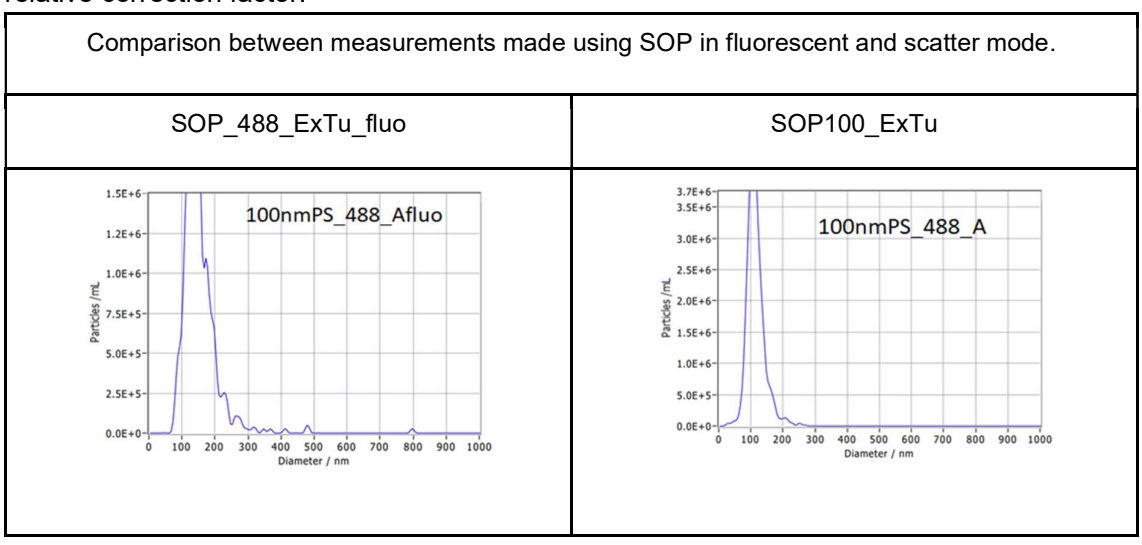
The relative correction factor for each sample was then calculated by dividing the concentration obtained in the 2<sup>nd</sup> measurement (scatter mode) by the concentration obtained in the 1<sup>st</sup> measurement (fluorescent mode). Then, the final relative correction factor was calculated as the average value of the results obtained for all samples. This relative correction factor was set then between the other parameters for future measurements using this SOP.

Table 35. Data of the measurements made for the calculation of the relative correction factor.

File name	SOP	Number of detected	Concentration measured	Relative	Diameter
File Hairie	304	particles	(particles/ml)	correction factor	(nm)
100nmPS_488_Afluo	SOP488_ExTu_fluo	77,4	3,5E+13	1.40	139,5
100nmPS_488_A	SOP100_ExTu	133,8	4,9E+13	1,40	106
100nmPS_488_Bfluo	SOP488_ExTu_fluo	67,4	3E+13	1,40	115,9
100nmPS_488_B	SOP100_ExTu	115,6	4,2E+13	1,40	115,8
100nmPS_488_Cfluo	SOP488 ExTu_fluo	77,2	3,5E+13	1.40	111,1
100nmPS_488_C	SOP100_ExTu	133,4	4,9E+13	1,40	115,6
100nmPS_488_Dfluo	SOP488 ExTu_fluo	69,6	3,1E+13	1,55	115
100nmPS_488_D	SOP100_ExTu	133,1	4,8E+13	1,55	116,6
100nmPS 488 Efluo	SOP488 ExTu fluo	115,8	5,2E+13	1,58	114,2
100nmPS_488_E	SOP100_ExTu	225	8,2E+13	1,56	120,9
100nmPS_488_Ffluo	SOP488_ExTu_fluo	91,6	4,1E+13	1,56	128,8
100nmPS_488_F	SOP100 ExTu	174,9	6,4E+13	1,50	114,3
100nmPS_488_Gfluo	SOP488 ExTu_fluo	86	3,9E+13	1,59	122,1
100nmPS_488_G	SOP100_ExTu	169,1	6,2E+13	1,59	122,8
100nmPS_488_Hfluo	SOP488_ExTu_fluo	70,8	3,2E+13	1,63	115,3
100nmPS_488_H	SOP100_ExTu	142,4	5,2E+13	1,03	120
100nmPS_488_Ifluo	SOP488_ExTu_fluo	70,3	3,2E+13	1,53	120,7
100nmPS 488 I	SOP100 ExTu	134,2	4,9E+13	1,55	126,6
100nmPS_488_Jfluo	SOP488_ExTu_fluo	83,8	3,8E+13	1 27	116
100nmPS_488_J	SOP100_ExTu	143,1	5,2E+13	1,37	120
100nmPS_488_Kfluo	SOP488 ExTu_fluo	62,1	2,8E+13	1,57	118
100nmPS_488_K	SOP100_ExTu	121,6	4,4E+13	1,57	115,4
100nmPS_488_Lfluo	SOP488 ExTu_fluo	70,8	3,2E+13	1,50	122
100nmPS_488_L	SOP100_ExTu	130,6	4,8E+13	1,50	119,4
100nmPS_488_Mfluo	SOP488_ExTu_fluo	65,1	2,9E+13	1.66	116,2
100nmPS_488_M	SOP100_ExTu	133,5	4,8E+13	1,00	123,2
Mean>				1,52	
SD>				0,09	

Table 35: As it is shown, each sample was measured twice: firstly, using the SOP established in fluorescent mode and then in the scatter mode. The relation between the concentration measured with the scatter and fluorescent mode and then the relative correction factor for SOP488\_ExTu\_fluo was obtained as the average of those results and set in the instrument for further measurements using that SOP.

Table 36. Size distribution histograms in Fluorescent - Scatter mode for the calculation of the relative correction factor.



# 2.3 Measurement of synthetic vesicles of different fluorophores densities.

Synthetic EVs (SEVs) from the 89-93-88nm range were measured. Considering that the three samples have similar sizes and stock concentrations (given by the supplier), SEVs of 88nm synthetic EVs (Stock concentration: 7,1E12) were the first evaluated, to calculate the final dilution since these SEVs have a fluorophores molar ratio 0%. For each sample introduced in the machine, two measurements were made as previously using SOP488\_ExTu\_fluo and SOP100\_ExTu. The final dilution used was 1:100000. Then, synthetic vesicles of 93nm (SEV93nm) were measured in the same conditions. These SEVs have a 0.1% fluorophores molar ratio and a concentration of 7.2E+12, both given by the provider. Finally, the measurement of SEV 88 nm was made under the same conditions. The concentration given by the provider was 7.1E+12 and these vesicles have 1% fluorophores molar ratio. Each sample was first measured using SOP488\_ExTu\_fluo and SOP100\_ExTu.

As was expected, since SEVs of 89nm have 0% molar ratio fluorophores, their measurement was not possible using SOP488\_ExTu\_fluo because the particles were not detected and all the positions in each measurement were excluded. Interestingly, the same results were obtained when using SOP488\_ExTu\_fluo for the measurement of 93nm SEVs, with 0.1% molar fluorophore ratio: SEVs were not sensed and therefore neither the concentration nor the size distribution could be calculated (Table 37). In contrast, the measurement of the 88nm SEVs could be carried out with both SOPs, even the mean concentration obtained with SOP488\_ExTu\_fluo was higher than that obtained with SOP100\_ExTu for each of the samples. The estimation of the size distribution was similar for both SOPs (Table 37).

As we can see, these SEVs with 0.1% fluorophores seem not to have enough fluorescent intensity to be measured using these SOP.

A possible pitfall in this experiment is that both the setting parameters of the final SOP488\_ExTu\_fluo and the calculation of the relative correction factor were carried out with polystyrene (PS) nanoparticles instead of SiO2. Considering that the SOP used to compare and thus calculate the relative correction factor was SOP100\_ExTu, which in turn was established by measurements with SiO2 nanoparticles and considering the differences between the refractive indices of PS and SiO2 and how this can affect the result of the NTA measurements, it would be interesting to add in future measurements with SiO2 nanoparticles and compare data.

Table 37. Example of size distribution histograms obtained after the measurement of the different SEVs, using SOP488 ExTu fluo and SOP100 ExTu SOP used Synthetic EVs evaluated SOP488 ExTu fluo SOP100 ExTu 89nm 5.5E+6-8.0E-1 5.0E+6 6.0E-1 4.5E+6 4.0E-1 Concentration: 4.0E+6-SEV89nm\_0\_SOPfluo\_U SEV89nm\_0\_SOP100\_U 2.0E-1 E 3.5F+6-7.1E+12 0.0E+0 3.0E+6 3.0E+6--2.0E-1 -4.0E-1 0% fluorophores 1.5E+6 -6.0E-1 molar ratio -8.0E-1 5.0E+5 -1.0E+0 100 150 200 250 300 350 400 100 150 200 250 300 350 400 450 SEVs were not sensed and therefore Concentration mean: 3.8E+12 neither concentration nor diameter were particles/mL SD: +/-4.4E11 measured. Diameter mean: 94.5nm SD: +/- 4.8 2.2E+6 93nm 2.0E+6 1.8E+6-1.8E+6-1.6E+6 1.6E+6-Concentration: 1.4E+6 1.4E+6-SEV93nm\_01\_SOPfluo\_11 SEV93nm 01 SOP100 11 7.2E+12 1.2E+6 1.2E+6 1.0E+6-1.0E+6 8.0E+5 8.0E+5-0.1% fluorophores 6.0F+5 6 0F+5 molar ratio 4.0E+5 4.0E+5-2.0E+5 100 200 300 400 500 600 700 800 900 1000 Concentration mean: 3E+12 particles/mL SEVs were not sensed and therefore SD: +/- 6E+11 neither concentration nor diameter were Diameter mean: 94.9nm measured. SD: +/- 2 88nm 5.5E+6-5.5E+6 5.0E+6-4.5E+6-5.0E+6-Concentration: 4.5E+6-₫ 4.0E+6-4.0E+6 7.1E+12 3.5E+6 3.5E+6 SEV88nm\_1\_SOP100\_10 SEV88nm\_1\_SOPfluo\_10 3.0E+6 2.5E+6 2.5E+6 2.0E+6 2.0E+6 1% fluorophores 1.5E+6 molar ratio 50 100 150 200 250 300 350 400 450 500 50 100 150 200 250 300 350 400 450 500 Concentration mean: 6.7E+12 Concentration mean: 8.2E+12 particles/mL particles/mL SD: +/- 7.6E+11 SD: +/- 8.5E+11 Diameter mean: 91.3nm Diameter mean: 92.6nm SD: +/- 2.9 SD: +/- 4

Our results show that the SOP set up for measurements in NTA fluorescence mode is sensitive to sense and analyze SEVs with a 1% molar ratio (it even seems to overestimate the concentration), but not sensitive enough to measure SEVs with a fluorophore molar ratio of 0.1%. In other words, the 88nm SEVs exhibit fluorescent intensity above the established SOP detection threshold, while the 93nm SEVs do not. Considering that all the particles evaluated in this experiment have similar concentrations and sizes, the results obtained support the fact

that the fluorescent mode of the NTA depends on the fluorescent intensity of the particle, regardless of the size or the concentration. To further confirm these results, future experiments should measure particles or EVs of a different size range, as well as evaluate the need to establish a new fluorescent mode SOP for the measurement of particles with a lower molar ratio of fluorophores. Table 37 shows the results of the measurements and a schematic representation of an example of the size distribution obtained.

## 3. Assessment of size determination by transmission electron microscopy (TEM)

The primary objective in this step is to estimate the size distribution of SiO2 nanoparticle samples by direct visualization using TEM. In addition, this technique helps us to corroborate the presence of vesicles in isolated samples. As previously mentioned, TEM is used to describe detailed structural features and additional information about the surface composition of EVs due to its nanometer scope and is the most widely used imaging methodology for the visualization and further characterization of EVs (Chuo et al. 2018).

It should be mentioned that obtaining EV images (and their quality) depends on the operator and the protocol used (Rikkert et al. 2019). To minimize this possible pitfall, the images were taken under the supervision of a second operator.

A total of 10 photos were taken in random regions of the grids for SiO2 nanoparticles of 100, 200, 300, and 400nm. Only 5 images of the 500nm particles could be taken, due to little material in the sample. Of the first four, 100 particles were analyzed at random, distributed in the 100 images, while only 66 particles were analyzed, which were all those found in the 5 photos taken.

Figure 11 shows representative examples of the images taken under TEM, in which it can be observe, different degrees of polydispersity in the samples of SiO2 nanoparticles of different diameters.

After performing the image obtention and processing, the results of size determination by TEM were compared with the size distribution by NTA. The comparison shows that the average diameter values obtained for each of the particles are substantially different between methods (Fig 12). When measuring 100nm particles, the average value using TEM is 79nm (SD +/- 9,8), while with NTA it is 97nm (SD +/- 1.84). In the evaluation of the 200 nm particles, the value obtained with NTA is 201nm (SD +/- 1), while with TEM it is 173.7nm (SD +/- 21). The values for the 300nm particles are 317 with TEM (SD +/- 97) and 247nm with NTA (SD +/- 3.48). When evaluating the 400nm particles: 430nm with TEM (SD +/- 68) and 375nm with NTA (SD +/- 18.37). Finally, the 500nm particles: 529nm with TEM (SD +/- 92) and 465nm with NTA (SD +/- 9.8).

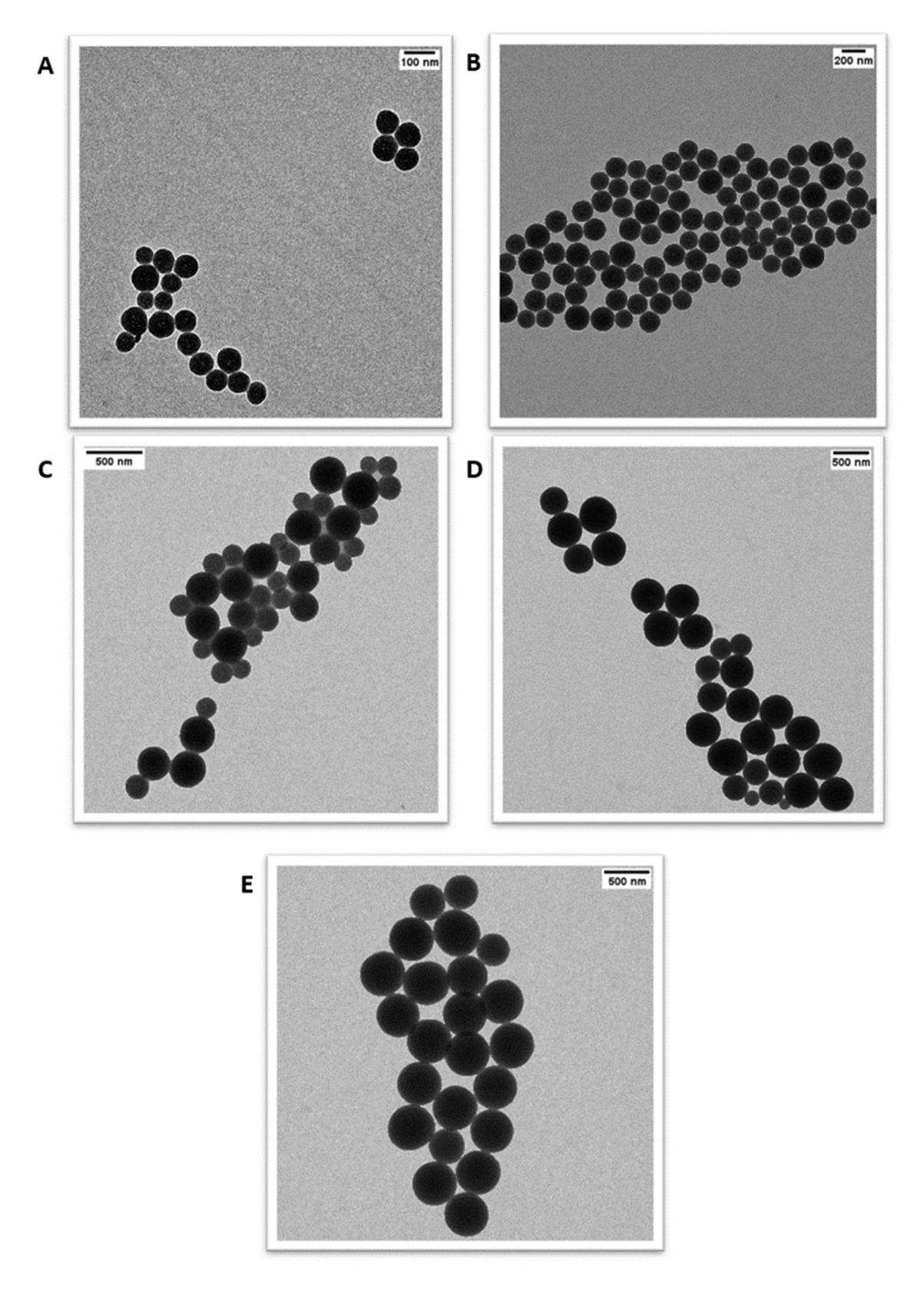


Figure 11: SiO2 nanoparticles images obtained under TEM. A: 100nm SiO2 nanoparticles. B: 200nm SiO2 nanoparticles. C: 300nm SiO2 nanoparticles. D: 400nm SiO2 nanoparticles. E: 500nm SiO2 nanoparticles.

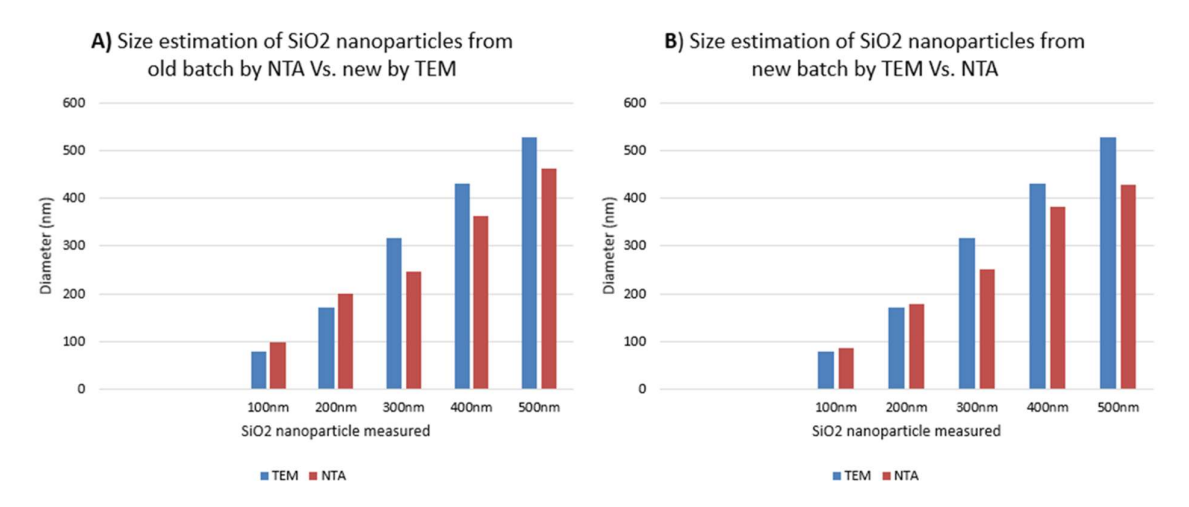


Figure 11: The graph illustrates the measurement of SiO2 particles of different sizes comparing the results obtained with TEM and NTA. A) TEM measurements of the new batch vs. NTA of the previous batch. B) Measurements with the same batch of particles in TEM and NTA.

It is worth mentioning, that the measurements made using NTA were with a different batch of nanoparticles than those used to visualize under TEM. This could explain the differences in the results. Unfortunately, it was not possible to measure the particles originally used in NTA under the microscope, so we performed new measurements with the LOT of new particles to compare the data. The results showed that the measurement using NTA of the particles from the new batch of 100nm was 85nm with an SD +/- 4.2nm (TEM: 79nm, SD +/- 9.8); 200nm: 179nm with an SD +/- 3.19nm (TEM: 173.7nm, SD +/- 21); 300nm: 251nm, SD: +/- 13.06nm (TEM: 317nm, SD +/- 97); 400nm: 382nm, SD: +/- 12.7nm (TEM: 430nm, SD +/- 68); and finally 500nm: 428nm, SD: +/- 16.5nm (TEM: 529nm, SD +/- 92). As we can see, the diameter of the smaller particles (100 and 200nm) was estimated with a greater similarity between both methods than the larger particles.

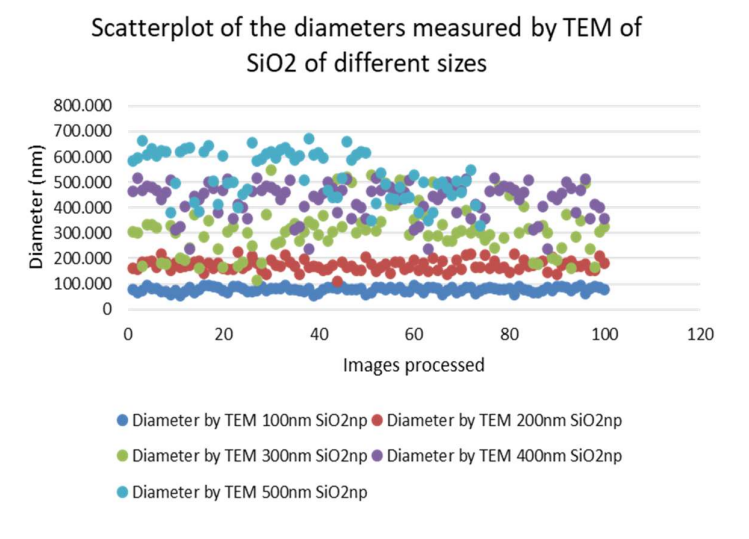


Figure 12: The graph shows the size of the measured particles Vs the number of analyzed particles. Great polydispersity is evident in the larger particles (mainly those of 300 and 400nm).

The second point that our results indicate is that there is a great polydispersity in the samples of larger particles, reflected by the higher value of SD in the measurement by all the methods. This polydispersity seems to be almost zero when evaluated in comparison with the 100 and 200 nm particles, as illustrated in Figure 12. The data also coincides with the findings of the measurement in NTA which is evidenced by the histograms of size distribution each time with a wider base as the size of the particle increases. This could explain the differences between both methods when evaluating the particles from the new batch.

Table 38. Results obtained by the assessment of size determination of SiO2 nanoparticles of different batches and sizes using NTA and TEM.

SiO2		Method							
nanoparticle	TEM new LOT		NTA Old LOT		NTA New LOT				
measured	Mean	SD	Mean SD		Mean	SD			
100nm	79	9,8	97,82	1,84	85	4,2			
200nm	172	21	201,01	1	179	3,19			
300nm	317	97	247,09	3,48	251	13,06			
400nm	431	68	363,07	18,37	382	12,7			
500nm	529	92	462,32	9.8	428	16,5			

Finally, the transmission electron microscopy evaluation of fraction 3 from SEC isolation and the EV large sample obtained by TFF isolation was performed. In Figure 13A, two clustered structures of about 150 nm in diameter are observed, which could correspond to an EV due to the apparent double membrane layer. On the other hand, in Figure 13B, a rounded particle of around 450 - 500 nm is observed, which although it does not present a clear double layer membrane, it presents associated structures that could correspond to blebs of a possible apoptotic body.

In our evaluation, the number of bilayer membrane structures was not sufficient to strongly conclude the presence of the vesicles of interest; this could be due to the low concentration and clustering of fractions during this evaluation.

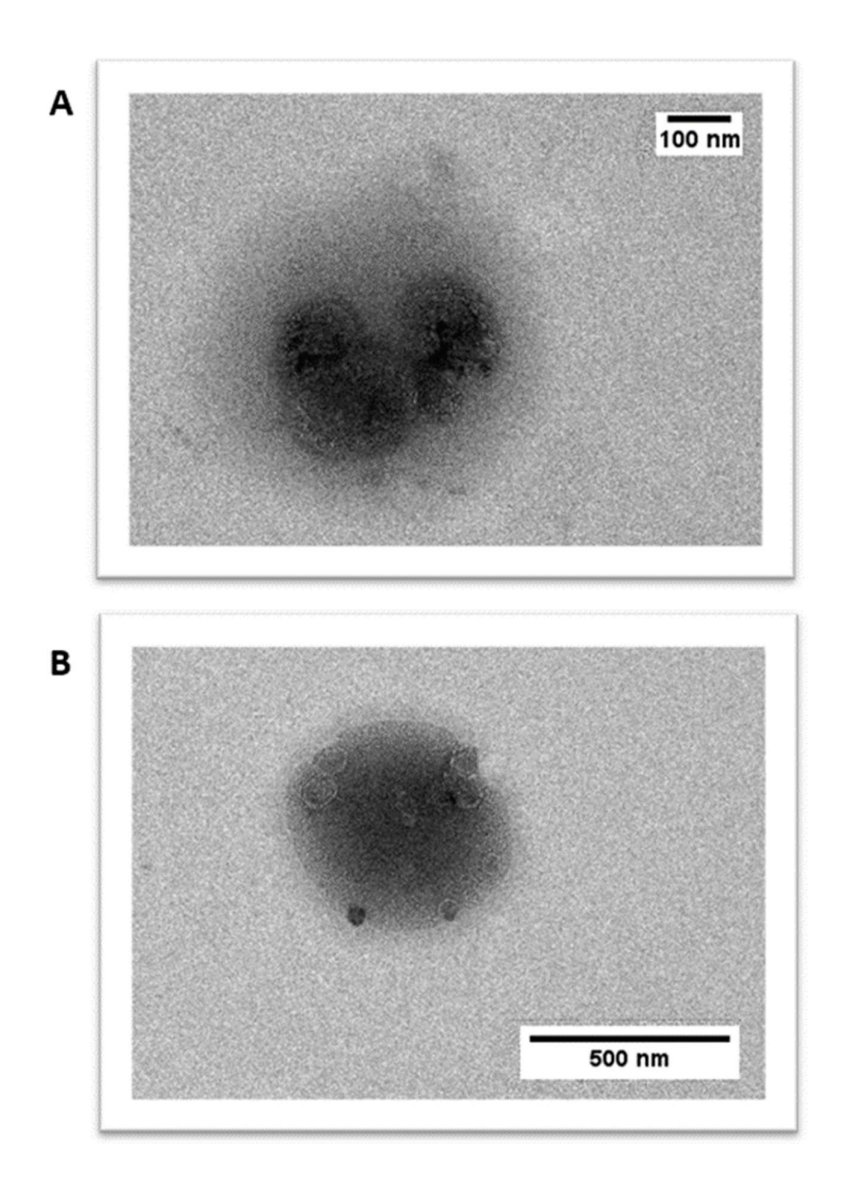


Figure 12: Direct visualization by TEM of: A) SEC fraction 3. B) EV large isolated by TFF.

### **CONCLUSIONS**

The field of extracellular vesicles (EVs) is an area of exponential and constant growth, as the physiological and pathophysiological functions are increasingly recognized. Clinical applications of EVs include their utility as diagnostic/prognostic markers for disease monitoring and treatment, drug delivery vehicles, and therapeutic vectors. Due to these crucially relevant potential applications, it may be obvious that the procedures for their characterization require standardization, since it is necessary to ensure the comparability of methods performed at different times, by different operators, in different laboratories.

Our results show that it is not possible to establish a single SOP in NTA and that in order to cover the measurement of the wide spectrum of EVs sizes found in biological samples, at least 3 SOPs are necessary: One that covers the size range smaller than 100nm (to be established in future experiments), one that covers particles from 100 to 300 nm (SOP100 ExTu), and one that covers larger particles, between 200 and 500nm (SOP500 ExTu). Unfortunately, the measurement of samples of different sizes of SiO2 nanoparticles in NTA could not be included in this work to evaluate in greater detail the resolution of the instrument when it comes to differentiating different populations and future experiments will be necessary in this regard. As expected, the measurements of a given diameter of SiO2 nanoparticles made with each SOP present different results, due to the different degree of sensitivity of the set parameters. However, it is worth mentioning that all the measurements made within each experiment showed almost zero variation. This lack of intra-experiment variation in our results supports the possibility of calculating the inter-experiment margin of error (or difference), which can help predict how far the measured results are from the expected/desired results. This lack of intraexperiment variation may allow, after exhaustive analysis, to predict the error/difference and establish a standardized protocol that finally allows the measurement of EVs in biological samples.

In addition to size and concentration analysis, NTA allows for the phenotyping of the particles under study using fluorescence-based measurements. As explained previously, this depends on the intensity of fluorescence and not on the size of the particle, as it was reflected in our results. Being able to establish standard operating procedures regarding the fluorescence threshold for the detection of labeled particles has important repercussions such as distinguishing EVs from non-EVs contaminants in a biological sample. This is of crucial importance for example in its potential application in liquid biopsy for diagnosis, prognosis, and monitoring of both disease and patient treatment.

Finally, the comparison of the results obtained in the determination of the size of the particles using NTA and TEM, we can conclude that the NTA measures with adequate precision the size distribution of the 100 and 200nm particles, while the larger particles presented more difficulties. On the one hand, this could mean that this technique has to improve its artificial

intelligence algorithms for the challenge of measuring large particles. On the other hand, this could be due to the stability or the mechanism of production and size determination of the SiO2 particles. Future experiments will be necessary to obtain definitive conclusions.

The work carried out in this thesis thoroughly evaluates the performance of the NTA to measure SiO2 nanoparticles and EVs, both in scatter mode and in fluorescent mode, providing valuable data that can be used for the generation of user guidelines for the standardization of the characterization of EVs.

### **REFERENCES**

- 1. Möller, A., & Lobb, R. J. (2020). The evolving translational potential of small extracellular vesicles in cancer. *Nature Reviews Cancer*, *20*(12), 697-709.
- 2. Nazarenko, I. (2020). Extracellular vesicles: Recent developments in technology and perspectives for cancer liquid biopsy. *Tumor Liquid Biopsies*, 319-344.
- 3. Welsh, J. A., van der Pol, E., Bettin, B. A., Carter, D. R., Hendrix, A., Lenassi, M., ... & Jones, J. C. (2020). Towards defining reference materials for measuring extracellular vesicle refractive index, epitope abundance, size, and concentration. *Journal of Extracellular Vesicles*, 9(1), 1816641
- Lázaro-Ibáñez, E., Sanz-Garcia, A., Visakorpi, T., Escobedo-Lucea, C., Siljander, P., Ayuso-Sacido, Á., & Yliperttula, M. (2014). Different gDNA content in the subpopulations of prostate cancer extracellular vesicles: apoptotic bodies, microvesicles, and exosomes. *The Prostate*, 74(14), 1379-1390.
- 5. Cai, J., Wu, G., Tan, X., Han, Y., Chen, C., Li, C., ... & Zeng, C. (2014). Transferred BCR/ABL DNA from K562 extracellular vesicles causes chronic myeloid leukemia in immunodeficient mice. *PloS one*, 9(8), e105200.
- Vestad, B., Llorente, A., Neurauter, A., Phuyal, S., Kierulf, B., Kierulf, P., ... & Øvstebø,
   R. (2017). Size and concentration analyses of extracellular vesicles by nanoparticle tracking analysis: a variation study. *Journal of extracellular vesicles*, 6(1), 1344087.
- 7. Varga, Z., Yuana, Y., Grootemaat, A. E., Van der Pol, E., Gollwitzer, C., Krumrey, M., & Nieuwland, R. (2014). Towards traceable size determination of extracellular vesicles. *Journal of extracellular vesicles*, *3*(1), 23298.
- 8. Nelson, B. C., Maragh, S., Ghiran, I. C., Jones, J. C., DeRose, P. C., Elsheikh, E., ... & Wang, L. (2020). Measurement and standardization challenges for extracellular vesicle therapeutic delivery vectors. *Nanomedicine*, *15*(22), 2149-2170.
- 9. Varga, Z., Van der Pol, E., Pálmai, M., Garcia-Diez, R., Gollwitzer, C., Krumrey, M., ... & Nieuwland, R. (2018). Hollow organosilica beads as reference particles for optical

- detection of extracellular vesicles. *Journal of Thrombosis and Haemostasis*, 16(8), 1646-1655.
- 10. Gardiner, C., Ferreira, Y. J., Dragovic, R. A., Redman, C. W., & Sargent, I. L. (2013). Extracellular vesicle sizing and enumeration by nanoparticle tracking analysis. *Journal of extracellular vesicles*, *2*(1), 19671.
- Bachurski, D., Schuldner, M., Nguyen, P. H., Malz, A., Reiners, K. S., Grenzi, P. C., ...
   Pogge von Strandmann, E. (2019). Extracellular vesicle measurements with nanoparticle tracking analysis—An accuracy and repeatability comparison between NanoSight NS300 and ZetaView. *Journal of extracellular vesicles*, 8(1), 1596016.
- Auger, C., Brunel, A., Darbas, T., Akil, H., Perraud, A., Bégaud, G., ... & Verdier, M. (2022). Extracellular Vesicle Measurements with Nanoparticle Tracking Analysis: A Different Appreciation of Up and Down Secretion. *International Journal of Molecular Sciences*, 23(4), 2310.
- 13. Van Der Pol, E., Coumans, F. A., Sturk, A., Nieuwland, R., & van Leeuwen, T. G. (2014). Refractive index determination of nanoparticles in suspension using nanoparticle tracking analysis. *Nano letters*, *14*(11), 6195-6201.
- Gardiner, C., Shaw, M., Hole, P., Smith, J., Tannetta, D., Redman, C. W., & Sargent,
   I. L. (2014). Measurement of refractive index by nanoparticle tracking analysis reveals
   heterogeneity in extracellular vesicles. *Journal of extracellular vesicles*, 3(1), 25361.
- Dragovic, R. A., Gardiner, C., Brooks, A. S., Tannetta, D. S., Ferguson, D. J., Hole, P., ... & Sargent, I. L. (2011). Sizing and phenotyping of cellular vesicles using Nanoparticle Tracking Analysis. Nanomedicine: Nanotechnology, Biology and Medicine, 7(6), 780-788.
- 16. Vogel, R., Savage, J., Muzard, J., Della Camera, G., Vella, G., Law, A., ... & Prina-Mello, A. (2021). Measuring particle concentration of multimodal synthetic reference materials and extracellular vesicles with orthogonal techniques: Who is up to the challenge?. *Journal of extracellular vesicles*, 10(3), e12052.
- 17. Yahata, S., Hirose, M., Ueno, T., Nagumo, H., & Sakai-Kato, K. (2021). Effect of Sample Concentration on Nanoparticle Tracking Analysis of Small Extracellular Vesicles and Liposomes Mimicking the Physicochemical Properties of Exosomes. Chemical and Pharmaceutical Bulletin, 69(11), 1045-1053.
- 18. Royo, F., Théry, C., Falcón-Pérez, J. M., Nieuwland, R., & Witwer, K. W. (2020). Methods for separation and characterization of extracellular vesicles: results of a worldwide survey performed by the ISEV rigor and standardization subcommittee. *Cells*, 9(9), 1955.
- 19. Xavier, Cristina P.R., Hugo R. Caires, Mélanie A.G. Barbosa, Rui Bergantim, José E. Guimarães, and M. H. Vasconcelos 2020. "The Role of Extracellular Vesicles in the

- Hallmarks of Cancer and Drug Resistance" Cells 9, no. 5: 1141. https://doi.org/10.3390/cells9051141
- Yokoi, A., & Ochiya, T. (2021, September). Exosomes and extracellular vesicles: Rethinking the essential values in cancer biology. In *Seminars in Cancer Biology* (Vol. 74, pp. 79-91). Academic Press.
- 21. Babaei, G., Vostakolaei, M. A., Bazl, M. R., Aziz, S. G. G., Gholipour, E., & Nejati-Koshki, K. (2022). The role of exosomes in the molecular mechanisms of metastasis: Focusing on EMT and cancer stem cells. *Life Sciences*, 121103.
- 22. Feng, L., Guo, L., Tanaka, Y., & Su, L. (2022). Tumor-Derived Small Extracellular Vesicles Involved in Breast Cancer Progression and Drug Resistance. *International Journal of Molecular Sciences*, *23*(23), 15236.
- 23. Battke, C., Ruiss, R., Welsch, U., Wimberger, P., Lang, S., Jochum, S., & Zeidler, R. (2011). Tumour exosomes inhibit binding of tumour-reactive antibodies to tumour cells and reduce ADCC. *Cancer immunology, immunotherapy*, *60*(5), 639-648.
- 24. Hellwinkel, J. E., Redzic, J. S., Harland, T. A., Gunaydin, D., Anchordoquy, T. J., & Graner, M. W. (2015). Glioma-derived extracellular vesicles selectively suppress immune responses. *Neuro-oncology*, *18*(4), 497-506.
- 25. Ciravolo, V., Huber, V., Ghedini, G. C., Venturelli, E., Bianchi, F., Campiglio, M., ... & Pupa, S. M. (2012). Potential role of HER2-overexpressing exosomes in countering trastuzumab-based therapy. *Journal of cellular physiology*, 227(2), 658-667.
- 26. Ye, J., & Liu, X. (2022). Interactions between endoplasmic reticulum stress and extracellular vesicles in multiple diseases. *Frontiers in Immunology*, 13.
- 27. Lin, C., Guo, J., & Jia, R. (2022). Roles of Regulatory T Cell-Derived Extracellular Vesicles in Human Diseases. *International Journal of Molecular Sciences*, *23*(19), 11206.
- 28. Ovchinnikova, L. A., Zalevsky, A. O., & Lomakin, Y. A. (2022). Extracellular Vesicles in Chronic Demyelinating Diseases: Prospects in Treatment and Diagnosis of Autoimmune Neurological Disorders. *Life*, *12*(11), 1943.
- 29. Anel, A., Gallego-Lleyda, A., de Miguel, D., Naval, J., & Martínez-Lostao, L. (2019). Role of exosomes in the regulation of T-cell mediated immune responses and in autoimmune disease. *Cells*, 8(2), 154.
- 30. lba, T., Levi, M., & Levy, J. H. (2022). Intracellular communication and immunothrombosis in sepsis. *Journal of Thrombosis and Haemostasis*, 20(11), 2475-2484.
- 31. Ståhl, A. L., Johansson, K., Mossberg, M., Kahn, R., & Karpman, D. (2019). Exosomes and microvesicles in normal physiology, pathophysiology, and renal diseases. *Pediatric Nephrology*, *34*(1), 11-30.

- 32. Zarà, M., Guidetti, G. F., Camera, M., Canobbio, I., Amadio, P., Torti, M., ... & Barbieri, S. S. (2019). Biology and role of extracellular vesicles (EVs) in the pathogenesis of thrombosis. *International journal of molecular sciences*, *20*(11), 2840.
- 33. Aguirre, R. S., Kulkarni, A., Becker, M. W., Lei, X., Sarkar, S., Ramanadham, S., ... & Mirmira, R. G. (2022). Extracellular vesicles in β cell biology: role of lipids in vesicle biogenesis, cargo, and intercellular signaling. *Molecular Metabolism*, 101545.
- 34. Lia, G., Di Vito, C., Cerrano, M., Brunello, L., Calcaterra, F., Tapparo, M., ... & Bruno, B. (2020). Extracellular vesicles after allogeneic hematopoietic cell transplantation: emerging role in post-transplant complications. *Frontiers in Immunology*, *11*, 422.
- 35. Liu, Z., Zhuang, Y., Fang, L., Yuan, C., Wang, X., & Lin, K. (2023). Breakthrough of extracellular vesicles in pathogenesis, diagnosis and treatment of osteoarthritis. *Bioactive Materials*, 22, 423-452.
- 36. Eguchi, A., Iwasa, M., & Nakagawa, H. (2022). Extracellular vesicles in fatty liver disease and steatohepatitis: role as biomarkers and therapeutic targets. *Liver International*.
- 37. He, C., Zheng, S., Luo, Y., & Wang, B. (2018). Exosome theranostics: biology and translational medicine. *Theranostics*, *8*(1), 237.
- 38. Yang, T., Martin, P., Fogarty, B., Brown, A., Schurman, K., Phipps, R., ... & Bai, S. (2015). Exosome delivered anticancer drugs across the blood-brain barrier for brain cancer therapy in Danio rerio. *Pharmaceutical research*, *32*(6), 2003-2014.
- Zhao, H., Yang, L., Baddour, J., Achreja, A., Bernard, V., Moss, T., ... & Nagrath, D. (2016). Tumor microenvironment derived exosomes pleiotropically modulate cancer cell metabolism. *elife*, 5, e10250.
- 40. Takakura, Y., Matsumoto, A., & Takahashi, Y. (2020). Therapeutic application of small extracellular vesicles (sEVs): pharmaceutical and pharmacokinetic challenges. *Biological and Pharmaceutical Bulletin*, *43*(4), 576-583.
- 41. Cooper, J. M., Wiklander, P. O., Nordin, J. Z., Al-Shawi, R., Wood, M. J., Vithlani, M., ... & Alvarez-Erviti, L. (2014). Systemic exosomal siRNA delivery reduced alphasynuclein aggregates in brains of transgenic mice. Movement Disorders, 29(12), 1476-1485.
- 42. Ohno, S. I., Takanashi, M., Sudo, K., Ueda, S., Ishikawa, A., Matsuyama, N., ... & Kuroda, M. (2013). Systemically injected exosomes targeted to EGFR deliver antitumor microRNA to breast cancer cells. *Molecular Therapy*, *21*(1), 185-191.
- 43. Arrighetti, N., Corbo, C., Evangelopoulos, M., Pastò, A., Zuco, V., & Tasciotti, E. (2019). Exosome-like nanovectors for drug delivery in cancer. *Current medicinal chemistry*, *26*(33), 6132-6148.

- 44. Tang, T. T., & Liu, B. C. (2019). Extracellular vesicles: opportunities and challenges for the treatment of renal fibrosis. *Renal Fibrosis: Mechanisms and Therapies*, 693-709.
- 45. Haney, M. J., Klyachko, N. L., Zhao, Y., Gupta, R., Plotnikova, E. G., He, Z., ... & Batrakova, E. V. (2015). Exosomes as drug delivery vehicles for Parkinson's disease therapy. *Journal of controlled release*, *207*, 18-30.
- Mizrak, A., Bolukbasi, M. F., Ozdener, G. B., Brenner, G. J., Madlener, S., Erkan, E. P., ... & Saydam, O. (2013). Genetically engineered microvesicles carrying suicide mRNA/protein inhibit schwannoma tumor growth. *Molecular Therapy*, 21(1), 101-108.
- 47. Wolf, P. (1967). The nature and significance of platelet products in human plasma. British journal of hematology, 13(3), 269-288.
- 48. Yáñez-Mó, M., Siljander, P. R. M., Andreu, Z., Bedina Zavec, A., Borràs, F. E., Buzas, E. I., ... & De Wever, O. (2015). Biological properties of extracellular vesicles and their physiological functions. *Journal of extracellular vesicles*, *4*(1), 27066.
- 49. Chargaff, E., & West, R. (1946). The biological significance of the thromboplastic protein of blood. *J Biol Chem*, *166*(1), 189-197.
- 50. Saveyn, H., De Baets, B., Thas, O., Hole, P., Smith, J., & Van Der Meeren, P. (2010). Accurate particle size distribution determination by nanoparticle tracking analysis based on 2-D Brownian dynamics simulation. *Journal of colloid and interface science*, 352(2), 593-600.
- 51. Qian, H., Sheetz, M. P., & Elson, E. L. (1991). Single particle tracking. Analysis of diffusion and flow in two-dimensional systems. *Biophysical journal*, *60*(4), 910-921.
- 52. Al-Khafaji, M. A., Gaál, A., Wacha, A., Bóta, A., & Varga, Z. (2020). Particle size distribution of bimodal silica nanoparticles: A comparison of different measurement techniques. *Materials*, *13*(14), 3101.
- 53. Brennan, K., Martin, K., FitzGerald, S.P. et al. A comparison of methods for the isolation and separation of extracellular vesicles from protein and lipid particles in human serum. Sci Rep 10, 1039 (2020). https://doi.org/10.1038/s41598-020-57497-7
- 54. Chuo, S.TY., Chien, J.CY. & Lai, C.PK. Imaging extracellular vesicles: current and emerging methods. J Biomed Sci 25, 91 (2018). https://doi.org/10.1186/s12929-018-0494-5
- 55. Rikkert, L G et al. "Quality of extracellular vesicle images by transmission electron microscopy is operator and protocol dependent." Journal of extracellular vesicles vol. 8,1 1555419. 9 Jan. 2019, doi:10.1080/20013078.2018.1555419